BNL-227979-2025-JAAM

Palm oil deoxygenation with glycerol as a hydrogen donor for renewable fuel production using nickel-molybdenum catalysts: The effect of support

N. Hongloi, L. Zhang

To be published in "Fuel Processing Technology"

June 2025

Center for Functional Nanomaterials

Brookhaven National Laboratory

U.S. Department of Energy

USDOE Office of Science (SC), Basic Energy Sciences (BES). Scientific User Facilities (SUF)

DISCLAIMER

Fuel Processing Technology 270 (2025) 108196

Contents lists available at ScienceDirect

Fuel Processing Technology

journal homepage: www.elsevier.com/locate/fuproc

Palm oil deoxygenation with glycerol as a hydrogen donor for renewable fuel production using nickel-molybdenum catalysts: The effect of support

Nitchakul Hongloi [a,b], Tawsif Rahman [b], Farshad Feyzbar-Khalkhali-Nejad [b], Chaiwat Prapainainar [c], Peerawat Wongsurakul [d], Emmanuel Aransiola [e], Lihua Zhang [f], Pascal Bargiela [g], Jonas Baltrusaitis [e], Paweena Prapainainar [a,**], Sushil Adhikari [b,h,*]

[a] National Center of Excellence for Petroleum, Petrochemicals and Advance Material, Department of Chemical Engineering, Faculty of Engineering, Kasetsart University, Bangkok 10900, Thailand
[b] Biosystems Engineering Department, 200 Corley Building, Auburn University, Auburn, AL 36849, USA
[c] Department of Chemical Engineering, Faculty of Engineering, King Mongkut's University of Technology North Bangkok, Bangsue, Bangkok 10800, Thailand
[d] Department of Chemical Engineering, Faculty of Engineering and Industrial Technology, Silpakorn University, Nakhon Pathom 73000, Thailand
[e] Department of Chemical and Biomolecular Engineering, Lehigh University, 111 Research Dr., Bethlehem, PA 18015, USA
[f] Brookhaven National Laboratory, Center for Functional Nanomaterials, Upton, NY 11973, USA
[g] Universite de Pau et des Pays de l'Adour, E2S UPPA, CNRS, IPREM, Pau, France
[h] Center for Bioenergy and Bioproducts, 520 Devall Drive, Auburn University, Auburn, AL 36849, USA

ARTICLE INFO

Keywords:
Biofuels
Hydrogen donor
Deoxygenation
$NiMo/Al_2O_3$
NiMo/HZSM-5

ABSTRACT

Palm oil, one of the most widely used vegetable oils, offers significant potential as a sustainable feedstock for biofuel production. This study explores the deoxygenation of palm oil using glycerol as a hydrogen donor, with nickel-molybdenum (NiMo) catalysts supported on commercial alumina (Al_2O_3), and zeolite (HZSM-5) comparing with self-prepared zirconia (ZrO_2). The catalysts were synthesized via incipient wetness impregnation and evaluated for their performance in biofuel production. $NiMo/Al_2O_3$ exhibited the lowest oxygen removal efficiency (68.5 %), while NiMo/HZSM-5 achieved a higher oxygen removal (74.3 %) but also demonstrated the highest coke formation. The type of support material influenced the resulting biofuel range, with NiMo/HZSM-5 and $NiMo/ZrO_2$ favoring jet fuel production, whereas $NiMo/Al_2O_3$ was more suitable for diesel production. Notably, $NiMo/ZrO_2$ exhibited the highest performance in palm oil deoxygenation while minimizing coke formation. These findings highlight $NiMo/ZrO_2$ as a promising catalyst for efficient and stable biofuel production, with the support material significantly influencing product yield and fuel quality.

1. Introduction

Fossil fuels have played a crucial role in global development across various sectors. However, their use has caused significant environmental challenges, particularly through greenhouse gas emissions and their effects on climate stability [1]. To address these issues, advancing alternative fuels is vital for reducing emissions and decreasing reliance on finite resources of fossil fuels. These alternative fuels, which encompass any fuel other than conventional fossil fuels, are often derived from renewable resources, including biomass, and typically have a lower environmental impact. Biofuels are considered carbon-neutral because the carbon dioxide (CO_2) released during combustion is balanced by the CO_2 absorbed by plants through photosynthesis [2]. Consequently, biofuels are increasingly important and crucial in sustainable energy solutions.

Biofuels are renewable energy from organic materials, such as agricultural waste, vegetable oil, or animal fats. They can serve as alternatives to traditional fossil fuels in transportation. The deoxygenation of oxygen-containing molecules is an effective process for producing alkane-based components, which are similar to conventional fossil fuels [3]. Deoxygenation involves several pathways, including decarbonylation, decarboxylation, and hydrodeoxygenation [4]. Deoxygenation of C_{16} or C_{18} oxygen-containing feedstocks produces alkane hydrocarbons in the diesel range, resulting in green diesel. Further cracking

* Corresponding author at: Auburn University, Auburn, AL 36849, USA.
** Corresponding author at: Kasetsart University, Bangkok 10900, Thailand.
E-mail addresses: fengpwn@ku.ac.th (P. Prapainainar), sushil.adhikari@auburn.edu (S. Adhikari).

https://doi.org/10.1016/j.fuproc.2025.108196
Received 2 December 2024; Received in revised form 5 February 2025; Accepted 19 February 2025
Available online 28 February 2025

reactions can generate lighter hydrocarbons similar to gasoline and jet fuel [5,6]. The effectiveness of both deoxygenation and cracking reactions is influenced by several factors, particularly the catalyst used. Most studies have focused on noble metal catalysts, including palladium (Pd), platinum (Pt), and ruthenium (Ru), for deoxygenation due to their high activity and selectivity in oxygen removal from feedstock [7]. However, these metals are costly for industrial applications. As a result, non-noble metals such as nickel (Ni), copper (Cu), molybdenum (Mo), and cobalt (Co) are becoming more prominent for deoxygenation. Hachemi et al. (2016) investigated the catalytic hydrodeoxygenation of stearic acid at 300 °C and 30 bar H_2 pressure using 5 wt% Ni on zeolite H-Y-80, 5 wt% Ni on γ-Al_2O_3, and 5 wt% Pd on carbon(C) catalysts. The stearic acid conversion was 100 % for both Ni/H-Y-80 and Ni/γ-Al_2O_3, while the Pd/C catalyst achieved only 53.74 %. The primary products were n-heptadecane ($C_{17}H_{36}$) and n-octadecane ($C_{18}H_{38}$), with varying selectivity among the catalysts. The Pd/C catalyst demonstrated lower activity compared to the Ni-based catalysts, producing a smaller proportion of alkanes and more intermediates. When the feedstock was changed to fatty acid methyl esters (FAME), tall oil fatty acid (TOFA), and animal fat, the Ni-based catalysts continued to outperform the Pd/C catalyst, achieving over 97.5 % feedstock conversion with C_{15} to C_{18} alkanes as the major products [8]. This comparison highlights the effectiveness of Ni-based catalysts in biofuel production over noble Pd/C catalysts. To enhance the performance of Ni in deoxygenation, the addition of a promoter is proposed. Among the various transition metals, Mo is widely used because it can improve Ni distribution by reducing Ni agglomeration and creating a synergistic effect between Ni and MoO_x [9]. This synergistic effect may further enhance the catalyst's performance in deoxygenation. Yang et al. (2022) studied the effect of Ni, Mo, and NiMo on $MgAl_2O_4$ for methyl palmitate hydrodeoxygenation. The bimetallic NiMo/$MgAl_2O_4$ catalyst exhibited higher performance than either monometallic catalyst. This enhanced performance was attributed to electron transfer between Ni and MoO_x due to d-d orbital overlap [10]. In the context of sustainable biofuel production, the traditional noble metal catalysts, such as Pt, Pd, and Ru, are known for their high activity and selectivity but are economically unviable for large-scale applications due to their scarcity and high cost. In contrast, non-noble metal catalysts, such as NiMo, supported on cost-effective materials, present an attractive alternative.

The feedstock type is also related to the sustainability of the biofuel production process, as it influences resource utilization, long-term environmental impact, and the composition of the biofuel product. The carbon number of the feedstock determines the carbon number of the liquid product. For example, palmitic acid has 16 carbon atoms, and its deoxygenation will result in a liquid product containing C15 and C16 carbon atoms from DCO/DCO_2 and HDO, respectively [11]. Triglycerides, the main components in vegetable oils and animal fats, are composed of various fatty acids with different carbon numbers, allowing them to produce alkanes across a range of fuel types. Over the past two decades, palm oil production has steadily increased to approximately one-third of the total vegetable oil produced globally [12]. Therefore, palm oil is suitable for producing renewable fuel due to its availability. Deoxygenation typically occurs under high initial hydrogen pressures between 20 and 50 bars [4]. The use of hydrogen donors is often preferred over external hydrogen because it simplifies operation, reduces costs, and avoids the need for high-pressure hydrogen gas. Various types of substances can act as hydrogen donors, including alcohols, acids, and other organic molecules [13]. It can generate hydrogen through decomposition and aqueous phase reforming (APR) [14,15]. Unlike other hydrogen donors, where alcohols can react with free fatty acids to form alkyl esters as side products [16], and acids can negatively impact the environment, glycerol is favored for deoxygenation because of its minimal side reactions, low cost, availability, and environmental advantages.

In our previous study, we investigated the effects of reaction temperature, time, and the activation method of a self-prepared NiMo/ZrO_2 catalyst—via either reduction or reduction and sulfidation—on palm oil deoxygenation using glycerol as a hydrogen donor. The results showed that higher reaction temperatures and longer reaction times led to increased oxygen removal and alkane selectivity. The sulfidation method outperformed the reduction in palm oil deoxygenation, likely due to the synergistic effects between Ni with ZrO_2 and Ni with MoS_2. Moreover, sulfidation improved the stability of the NiMo/ZrO_2 catalyst, resulting in reduced coke formation [17].

Al_2O_3, a widely available and cost-effective material, possesses moderate acidity, making it ideal for green diesel production. HZSM-5, a zeolite with strong acidity and a distinctive pore structure, facilitates cracking reactions and supports the production of lighter alkanes, such as jet fuel and gasoline. These supports not only enhance catalyst performance but also contribute to the sustainability of the process by reducing dependence on scarce materials and improving the efficiency of biofuel production. However, the primary limitations of Al_2O_3 as a catalyst include its deactivation due to water absorption [18], and HZSM-5's susceptibility to coke formation [19], resulting in reduced catalytic efficiency and a short lifespan that necessitates frequent regeneration, thereby increasing production costs. By leveraging the properties of these supports, our study aims to investigate the performance and stability of these materials, identifying viable pathways for the economic and environmental advancement of renewable energy technologies.

Therefore, this study aims to compare the performance of our self-prepared NiMo/ZrO_2 catalyst with a commercial catalyst, specifically NiMo, on Al_2O_3 and HZSM-5, both of which are widely used in industrial hydroprocessing [20]. The sulfidation method was selected for catalyst activation, with reactions carried out at 400 °C for 1 and 3 h. The catalysts were characterized using several techniques, including Fourier transform infrared spectroscopy (FTIR), x-ray diffraction (XRD), scanning electron microscopy (SEM), scanning transmission electron microscopy (STEM), x-ray photoelectron spectroscopy (XPS), nitrogen sorption, and thermogravimetric analysis (TGA). Liquid and gas products were collected, and the liquid products were analyzed using gas chromatography–mass spectrometry (GC–MS), elemental analysis, total acid number (TAN), high heating value (HHV), and Simulated distillation (Simdist). All data relating to the NiMo/ZrO_2 catalyst (reduced and sulfided) performance presented in this manuscript are derived from our previous publication [17] and have been included here solely for comparative purposes. While previous studies have investigated biofuel production through deoxygenation, most research has focused on either noble metal catalysts or single-support NiMo catalysts, with limited direct comparisons of different supports under identical reaction conditions. This study advances the field by evaluating the performance of NiMo catalysts supported on both self-prepared and commercial materials for palm oil deoxygenation, utilizing glycerol as an in-situ hydrogen donor. By assessing reaction performance, catalyst stability, and biofuel properties, this study provides valuable insights into the influence of catalyst supports on optimizing biofuel production. Moreover, the use of glycerol—a byproduct of biodiesel production—as a hydrogen donor presents a sustainable alternative to conventional hydrogen gas-based hydrodeoxygenation, thereby reducing process complexity and operational costs. The findings offer a practical framework for selecting cost-effective and efficient catalyst systems, contributing to the advancement of large-scale renewable fuel production.

2. Materials and method

2.1. Materials

Zeolite ZSM-5 (ammonium form) with the SiO_2/Al_2O_3 ratio of 50:1, aluminum oxide (γ-phase, high surface area catalyst support bimodal (γ-Al_2O_3)), ammonium heptamolybdate tetrahydrate ≥99 % ($(NH_4)_6Mo_7O_{24}\cdot 4H_2O$), nickel (II) nitrate hexahydrate 98 % ($Ni(NO_3)_2\cdot 6H_2O$), and 99 % eicosane ($C_{20}H_{42}$) were purchased from Thermo Scientific

Chemicals (Waltham, Massachusetts, USA). Glycerol with 99.5 % purity was obtained from VWR (Radnor, Pennsylvania, USA). Refined, bleached, and deodorized (RBD) palm oil, a yellow solid, was utilized as the reactant and purchased from Soapeauty Co. Ltd. (Des Plaines, Illinois, USA). The fatty acid composition in palm oil is provided in the previous study [17]. Dichloromethane (DCM) was purchased from Macron Fine Chemicals (Radnor, Pennsylvania, USA). Alkane standard solution C_8-C_{20} (C_8-C_{20}, ~40 mg/L each, in hexane) was purchased from Sigma Aldrich (St. Louis, Missouri, USA). High-purity nitrogen and hydrogen gases were obtained from Airgas Inc. (Opelika, Alabama, USA).

2.2. Catalyst preparation

Two commercial supports, HZSM-5 and Al_2O_3, were chosen for this study. Fourier transform infrared spectroscopy (FTIR) was employed to verify the bonding types of HZSM-5 and Al_2O_3 before loading with active metals. Metal salt reagents were measured to achieve 10 wt% Ni and 5 wt% Mo on the supports. Metals were introduced using the incipient wetness impregnation method, where metal reagent solutions were gradually added to the support. The resulting slurry was dried at 110 °C for 12 h, then calcined at 550 °C for 5 h. The catalysts were reduced before deoxygenation for 4 h at 500 °C in a tube furnace with a 10 ml/min flow of 10 % H_2 in N_2 to convert the metal oxides into their metallic forms.

2.3. Catalyst characterization

Detailed description of catalyst characterization using FTIR, XRD, SEM/EDS, STEM, N_2 sorption, and TGA are described in the published document elsewhere [17]. Chemical analysis of the supported catalyst surfaces was conducted using an Escalab 250 Xi XPS instrument. Monochromated Al Kα radiation (1486.6 eV) was used as the excitation source operating at 225 W with an X-ray beam spot size of 650 μm, and an electron flood gun was utilized to neutralize any charge during the acquisition process. A pass energy of 20 eV was used to acquire high-resolution spectra, while a pass energy of 120 eV was used for survey spectra. Binding energies for Al_2O_3 supported catalysts were corrected for charging by referencing the Al 2p peak at 74.5 eV [21]. For quantification, variation with the kinetic energy of the Effective Attenuation Length (EAL) was corrected as described by Seah et al. (2012) [22]. Scofield cross-sections were used [23], and inelastic background was accounted for using the Shirley method [24]. S 2 s and Mo 3d region (S2S + Mo3d) was fitted using synthetic components comprised of single-parameter Voigt function [25], LA(m), where *m* of 50 was used in all but components. Spin-orbit coupling was accounted for when constraining Mo $3d_{5/2}$ and Mo $3d_{3/2}$ components while the doublet splitting was set to 3.13 eV. The processing of the XPS spectra was performed with CasaXPS software [26].

2.4. Deoxygenation under glycerol as a hydrogen donor

A detailed description of the deoxygenation of palm oil using glycerol is discussed in the published document [17]. Briefly, 12 g of palm oil, 5 g of glycerol, and 0.5 g of reduced NiMo catalyst were added into the reactor, aligning with the stoichiometric requirements (the calculation is shown in the previous study [17]). For catalyst sulfidation, 0.4 ml of dimethyl disulfide was added to form NiMoS [17,27]. To remove the air inside the reactor, the N_2 was used to flush the reactor three times before the reaction. The reactions were conducted at 400 °C for 1 and 3 h once the desired temperature was achieved. The final pressure varied depending on the reaction conditions, ranging from 600 to 1100 psi. After the reaction, the reactor was allowed to cool to room temperature and then weighed. The liquid product was filtered to separate the catalyst. Each experiment was performed in duplicate.

2.5. Product analysis

The liquid product was filtered to separate the catalyst using Whatman No.50 filter paper, which has a particle filtration size of 2.7 μm. The filtered liquid was then prepared in solution for the GC–MS analysis. Additional analyses included CHNS-O, total acid number (TAN), higher heating value (HHV), and simulated distillation (SimDis). These techniques are explained in detail in a previously published document [28]. The results from GC–MS and CHNS-O were utilized to calculate the mass balance and other indicators using the equations provided below.

$$\%\text{Liquid yield} = \frac{m_{final}}{m_{initial}} \times 100 \quad (1)$$

$$\%\text{Carbon yield} = \frac{m_{C,product}}{m_{C,feed}} \times 100 \quad (2)$$

$$\%\text{Alkane selectivity} = \frac{mol_{\text{alkane hydrocarbon in liquid product}}}{mol_{\text{total of liquid product}}} \times 100 \quad (3)$$

$$\%\text{Oxygen removal} = \frac{m_{O,feed} - m_{O,product}}{m_{O,feed}} \times 100 \quad (4)$$

where $m_{initial}$ = mass of all substances at initial (g)
m_{final} = mass of all substances after reaction (g)
$m_{C,feed}$ = mass carbon in feed (g).

The performance indicators selected in this study—alkane selectivity, oxygen removal, carbon yield, TAN, and HHV—are crucial for assessing the practical applicability of biofuel production processes. Alkane selectivity measures the catalyst's ability to convert oxygen-containing compounds, such as triglycerides and free fatty acids, into hydrocarbons suitable for transportation fuels. High alkane selectivity is essential to minimize undesirable byproducts and ensure the production of high-quality fuel fractions such as gasoline, jet fuel, and diesel. Oxygen removal is another critical indicator, as it determines the deoxygenation process necessary for producing hydrocarbons with higher heating values and improved stability. This also ensures fuel compatibility with existing engines, as residual oxygen can lead to corrosion and reduced combustion efficiency. Carbon yield quantifies the conversion of carbon from the feedstock into liquid hydrocarbons, with a high carbon yield minimizing losses to gaseous or solid products, thus improving the economic feasibility of the process. TAN and HHV provide valuable insights into fuel quality and energy content. A low TAN signifies reduced acidity, which enhances fuel stability and decreases the likelihood of engine corrosion, while an increase in HHV indicates the successful conversion of oxygenates into energy-dense hydrocarbons, aligning the product with conventional fuel energy requirements. By focusing on these performance indicators, this study emphasizes the industrial relevance of NiMo catalysts and the potential of glycerol as a cost-effective, sustainable hydrogen donor, offering a framework for optimizing catalyst design and operational parameters for large-scale biofuel production.

3. Results and discussion

3.1. Catalyst characterization

3.1.1. FTIR

The bonding type of support was determined using FTIR, and the results are shown in Fig. 1. The transmittance peaks of γ-Al_2O_3 were observed at four main positions: 3420, 1640, 796, and 540 cm^{-1}. The first two peaks represented O—H stretching and bending vibrations in adsorbed water molecules, respectively. The peaks at 796 and 540 cm^{-1} are attributed to the vibrations of Al—O—Al [29].

HZSM-5 is a zeolite with framework vibration and surface properties generated from the SiO_2:Al_2O_3. The FTIR spectrum demonstrated the characteristics of these properties. There were seven major peaks in the

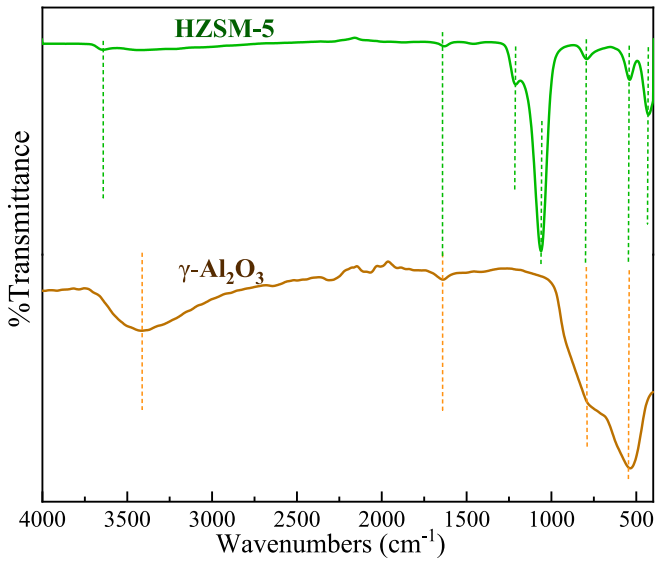

Fig. 1. FTIR spectrum of catalyst supports.

HZSM-5 spectrum: 3640, 1640, 1220, 1060, 796, 540, and 430 cm^{-1}. The small band at 3640 cm^{-1} indicates the hydroxyl group of the extra-framework alumina (Al—OH framework), which provides Brønsted acid sites. The bending vibration of water-adsorbing molecules in the framework corresponds to the band at 1640 cm^{-1}. The significant bands at 1220, 1060, and 796 cm^{-1} corresponded to the Si—O—Si external asymmetric, internal asymmetric, and external symmetric, respectively [30]. Thus, those peaks can confirm the presence of external linkages between the SiO_4 tetrahedral structure in zeolite. The absorption bands at 540 and 430 cm^{-1} indicate the HZSM-5 crystalline structure of SiO_4 and AlO_4 tetrahedral, also known as double five rings.

The FTIR spectrum alumina and HZSM-5 displayed characteristic peaks as expected. The absence of unknown peaks, along with the presence of the characteristic peaks, confirmed the purity of selected supports [30,31].

3.1.2. XRD

XRD analysis was performed to examine the characteristic peaks of the fresh and spent catalysts. Fig. 2(a) presents the XRD patterns of NiMo supported on Al_2O_3. Significant peaks in the XRD pattern of Al_2O_3 appeared at 2θ of 22°, 37°, 46°, and 66°, corresponding to the (111), (311), (400), and (440) planes, respectively. These peaks indicated the formation of the cubic and pure gamma phases of Al_2O_3 [32,33].

Fig. 2(b) shows the XRD patterns of NiMo supported on HZSM-5. The XRD pattern of HZSM-5, indicative of its MFI (Mobil Composition of Framework I) structure, was essential for identifying its crystalline structure. Dominant peaks for NiMo/HZSM-5 were observed within the 2θ range of 8–9 and 22–25°. The diffraction peaks at 8.0°, 8.9°, 23.1°, 23.3°, and 24°, corresponding to the (101), (200), (051), (303), and (313) planes, respectively. These results confirmed that NiMo/HZSM-5 exhibited an MFI-type zeolite structure [30,34].

A distinct nickel peak was observed in all catalysts, with NiO displaying peaks at 2θ = 43.3° related to the (200) planes and Ni exhibiting characteristic peaks at 2θ = 54°, corresponding to the (220) plane [35]. However, Mo species peaks were not detected, possibly due to their small crystalline size, resulting in a high dispersion of metal particles across all catalysts [36]. The XRD comparison of fresh and spent catalysts revealed that the diffraction peaks of the supports remained unchanged after the reaction, indicating that the structure of both supports remained stable throughout the process. For the Ni peak, the intensity decreased in all catalysts due to coke deposition, with a significant reduction observed in NiMo on HZSM-5. This result corresponds with the TGA analysis (see Section 3.1.7), which shows that NiMo on HZSM-5 exhibited higher coke formation compared to NiMo on Al_2O_3 [37]. The presence of Ni^{2+} may result from the weak interaction between Ni and the support, facilitating the reoxidation of nickel species upon contact with air. The satellite peak of Ni is associated with multielectron processes within Ni^{2+} compounds, such as NiO and $NiMoO_4$ alloys.

3.1.3. XPS

The chemical states on the surface of fresh and spent NiMo catalysts supported on Al_2O_3 and HZSM-5 were examined using XPS analysis. Fig. 3 presents the XPS spectra of Ni 2p and Mo 3d for various supports. Ni 2p region shows that the Ni state in the NiMo/HZSM-5 catalyst exhibits three overlapping peaks at binding energies of 853, 856, and 862 eV, corresponding to Ni^0, Ni^{2+}, and the satellite peak, respectively [38]. The presence of Ni^{2+} may result from the weak interaction between Ni and the support, facilitating the reoxidation of nickel species upon contact with air. The satellite peak of Ni is associated with multielectron processes within Ni^{2+} compounds, such as NiO and $NiMoO_4$ alloys [39].

The Mo states observed in the NiMo catalysts supported on Al_2O_3 and

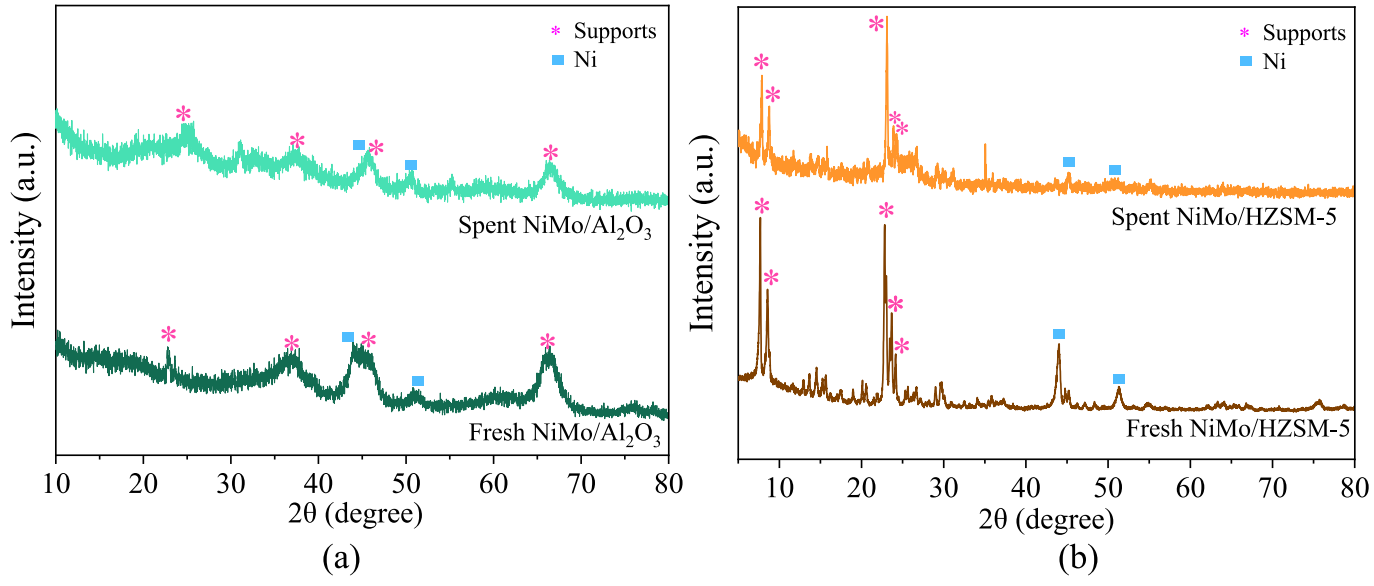

Fig. 2. XRD pattern of (a) NiMo/Al_2O_3 and (b) NiMo/HZSM-5.

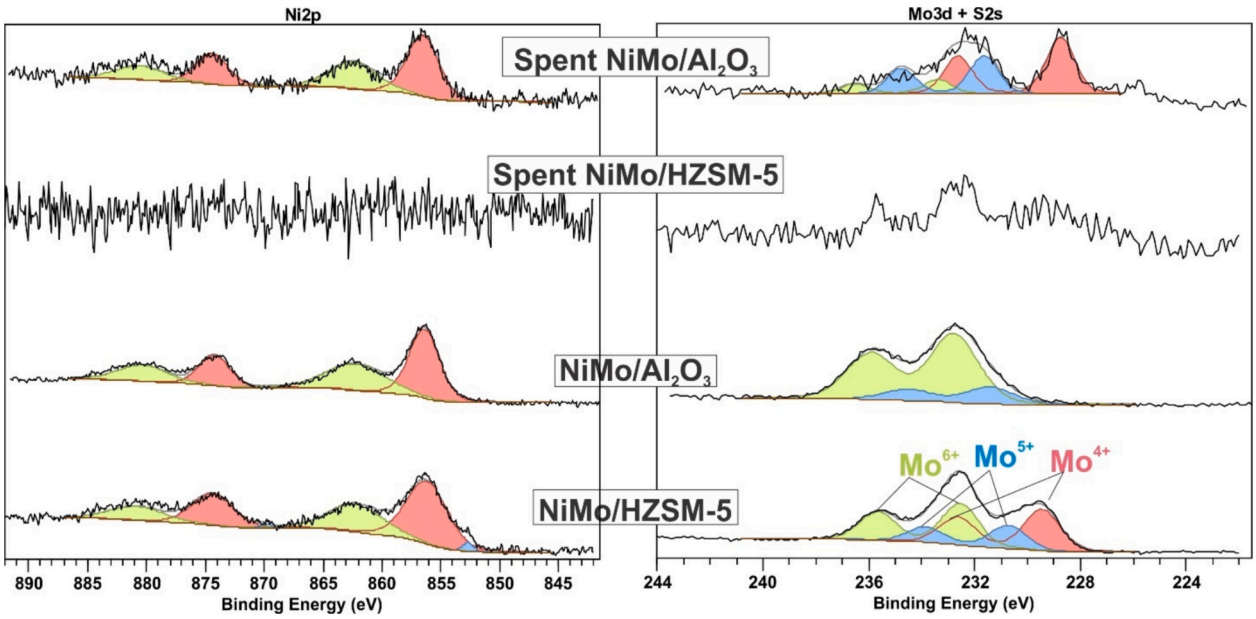

Fig. 3. XPS spectra of fresh catalyst; (a) Ni 2p and (b) Mo 3d.

HZSM-5 included Mo^{6+}, Mo^{5+}, and Mo^{4+} [40]. The binding energies for Mo^{6+} are represented by two peaks at 232.3 eV and 235.8 eV, corresponding to the $3d_{5/2}$ and $3d_{3/2}$, respectively. Peaks for Mo^{4+} appear at 229.5 eV and 232.6 eV, corresponding to the $3d_{5/2}$ and $3d_{3/2}$, suggesting the presence of MoO_2 along some intermediate Mo^{5+} species in NiMo/HZSM5, implying partial reduction to $NiMoO_x$. No metallic Mo was observed as the binding energy of Mo(0) $3d_{5/2}$ peak is typically at 227.8 eV.

Elemental quantification of fresh and spent catalyst surfaces is presented in Table 1. An interesting observation can be made where the catalyst surface is significantly modified during the reaction. In particular, spent NiMo/HZSM5 now contains 91 % of carbon, while spent $NiMo/Al_2O_3$ also contains a significant amount. Sulfur in both spent catalysts does not contribute significantly.

3.1.4. SEM-EDS

Fig. 4 presents the surface morphology and elemental composition of fresh and spent NiMo catalysts supported on Al_2O_3 and HZSM-5. Fig. 4 (a) shows the fresh $NiMo/Al_2O_3$ catalyst, characterized by a rough surface with irregularly shaped particles due to metal deposition. Elemental mapping revealed the distribution of Al in the Al_2O_3 support, while O in both the support and oxidized metals, and Ni and Mo across the catalyst surface. Ni and Mo were evenly distributed without significant aggregation. In Fig. 4(b), the spent $NiMo/Al_2O_3$ catalyst exhibited a highly textured surface with aggregated particles, where higher magnification revealed a granular structure. Coke deposition, indicated by the carbon map, suggested the presence of carbonaceous deposits that could block the catalyst's active sites.

Fig. 4(c) depicted the morphology of the fresh NiMo/HZSM-5 catalyst, indicating an uneven and aggregated structure. The even distribution of Al and Si confirmed the HZSM-5 zeolite structure, with the silica framework also evenly distributed, indicating a well-maintained zeolite structure. Ni and Mo were uniformly distributed across the catalyst, indicating effective preparation and deposition on the HZSM-5 support. Fig. 4(d) shows the SEM-EDS analysis of the spent NiMo/HZSM-5 catalyst, revealing significant morphological changes compared to the fresh catalyst. The surface had become rougher and more irregular, with larger clusters and signs of sintering or agglomeration, as confirmed by carbon mapping indicating carbon deposits.

Table 1
Elemental quantification of the fresh and spent catalyst surfaces.

Sample Identifier	Elemental quantification (%)						
	Al 2p	C 1 s	Mo 3d	Ni 2p	O 1 s	S 2p	Si 2p
Spent $NiMo/Al_2O_3$	12.6	61.9	0.3	0.6	23.7	0.9	0.0
Spent NiMo/HZSM-5	0.1	91.0	0.0	0.0	7.4	0.2	1.3
$NiMo/Al_2O_3$	31.9	7.3	1.2	2.5	57.0	0.0	0.0
NiMo/HZSM-5	1.6	16.2	2.1	1.6	54.1	0.0	24.5

3.1.5. STEM-EDS

The dark-field STEM images and EDS mappings of the catalysts are illustrated in Fig. 5. The dark-field STEM image reveals that the brighter regions correspond to denser NiMo particles, while the dimmer regions indicate the support material. In Fig. 5(a), the STEM-EDS analysis of $NiMo/Al_2O_3$ shows a well-dispersed Al content, implying that Al is evenly distributed within the support. Ni is also well-dispersed on the Al_2O_3 support with minimal aggregation, whereas Mo appears to be more uniformly dispersed than Ni.

Fig. 5(b) presents the STEM-EDS data for NiMo/HZSM-5, where the even distribution of Si and Al suggests that these elements are well-distributed within the support. Similar to $NiMo/Al_2O_3$, Ni is well-dispersed on the HZSM-5 support with limited aggregation, but Mo is more evenly dispersed than Ni. Notably, Ni shows a higher degree of aggregation on HZSM-5 compared to Al_2O_3. This corresponds to N_2 sorption results (see section 3.1.6), HZSM-5 exhibits a microporous structure, while Al_2O_3 displays a mesoporous structure. Consequently, NiMo could not effectively penetrate the micropores of HZSM-5, resulting in greater aggregation compared to Al_2O_3.

3.1.6. N_2 adsorption-desorption

Fig. 6 illustrates the N_2 adsorption-desorption isotherms for the supports, fresh and spent catalysts. Fig. 6(a) shows the isotherm for Ni on Al_2O_3. The results show that Al_2O_3 displays a type IV isotherm with an H2-type hysteresis loop, as classified by IUPAC [41]. This hysteresis loop is evident in the relative pressure (P/P^0) range of 0.50 to 0.95, indicating a mesoporous structure [42]. Fig. 6(b) depicts the isotherm for Ni on HZSM-5, which is a combination of type I and type IV adsorption isotherms. The H2-type hysteresis loop in HZSM-5 is observed between relative pressures of 0.5 and 1.0. The type I isotherm at low relative pressure ($P/P^0 = 0.04$) corresponded to the microporous

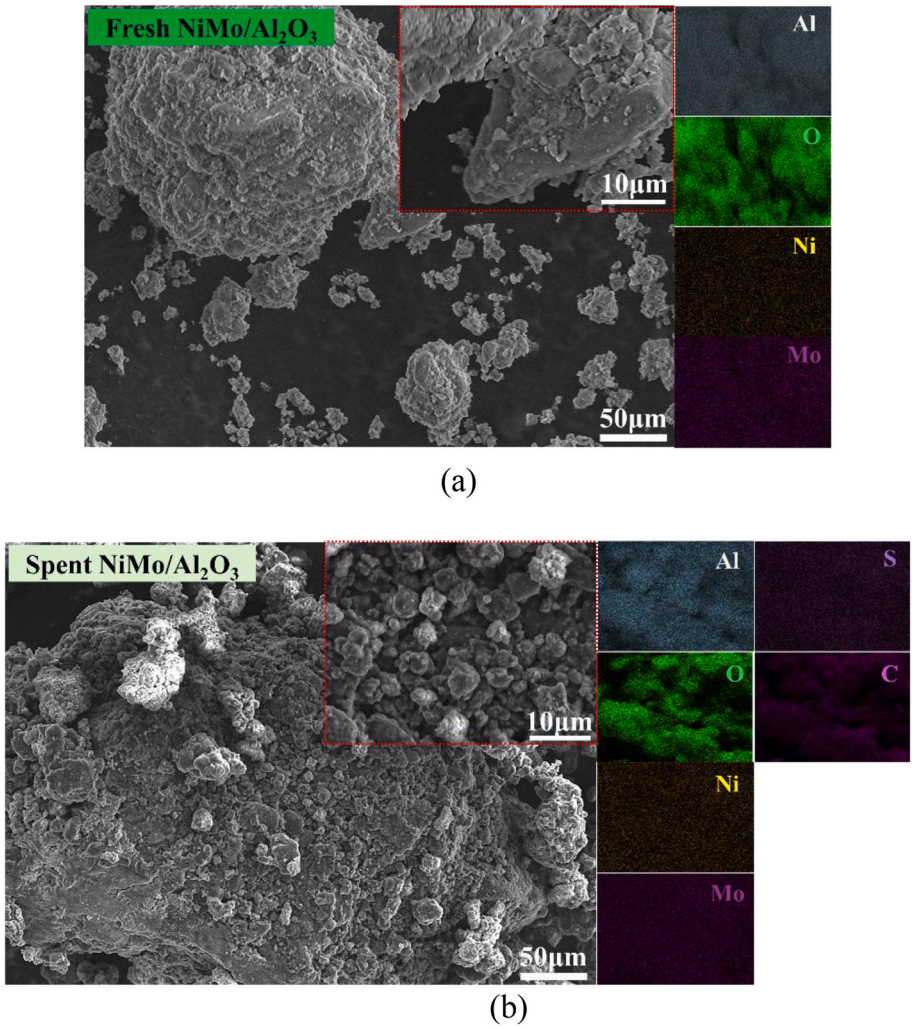

Fig. 4. SEM images of fresh and spent catalysts.

structure, while the type IV isotherm with H2-type hysteresis confirmed the mesoporous structure [43,44]. These findings were consistent with the BJH analysis (shown in Supplementary Information, Fig. S1), indicating that the pore size distribution of HZSM-5 is composed of micropores (below 0.2 nm) and mesopores structure, whereas Al_2O_3 only exhibits a mesoporous structure.

After metal loading, the N_2 adsorption of NiMo on Al_2O_3 and HZSM-5 decreased significantly compared to their bare support, suggesting that the introduction of NiMo may block some pores and decrease overall porosity corresponding with a decrease in BET surface area (as shown in Table 2) [45]. However, the type of adsorption isotherm and hysteresis loop remained unchanged, indicating that metal loading did not compromise the support structure [46]. For both NiMo on Al_2O_3 and HZSM-5, the spent catalysts showed a distinct decrease in adsorption amounts, particularly at higher relative pressures, suggesting pore blockage or structural changes due to coke formation after catalytic activity.

Table 2 summarizes the textural properties of the supports, fresh catalysts, and spent catalysts. HZSM-5 demonstrated a higher surface area than Al_2O_3, attributed to its microporous structure. After metal loading, both catalysts exhibited a decrease in surface area due to metal agglomeration and pore blockage, particularly in NiMo/HZSM-5, where micropore blockage was observed [47]. However, the surface area of NiMo/HZSM-5 remains higher than that of NiMo/Al_2O_3. Interestingly, the spent NiMo/HZSM-5 exhibited a lower surface area than the spent NiMo/Al_2O_3, indicating greater coke formation on NiMo/HZSM-5, which aligns with the TGA results (Fig. 7).

3.1.7. TGA

Fig. 7 presents the TGA profiles of fresh and spent catalysts supported on ZrO_2, Al_2O_3, and HZSM-5. The TGA analysis reveals distinct weight loss trends for each catalyst, highlighting differences in their stability and coke formation. Fresh catalysts experienced minimal weight loss of approximately 5 % for NiMo on Al_2O_3, and HZSM-5 (with their curves overlapping after 200 °C), mainly due to moisture evaporation. However, spent catalysts showed significant weight loss, indicating coke deposition during the deoxygenation process. Previous experiments with spent NiMo/ZrO_2 catalysts under the same conditions showed a coke deposition of 15 % weight loss [17]. TGA results for commercial catalysts (NiMo/Al_2O_3 and NiMo/HZSM-5) revealed that decomposition temperature can be divided into three phases: below 200 °C is physical processes such as the release of volatile compounds or water evaporation; between 200 and 450 °C, where NiMo sulfides decompose and residual hydrocarbons combust to form soft coke, which may block active sites and lead to deactivation; and above 450 °C, where hard coke decomposes, presenting a more persistent challenge to maintaining catalyst activity [48].

For the fresh NiMo/Al_2O_3 and NiMo/HZSM-5 catalysts, the weight loss was approximately 5 %, likely due to water absorption. However, the spent catalysts demonstrated higher weight losses, reflecting

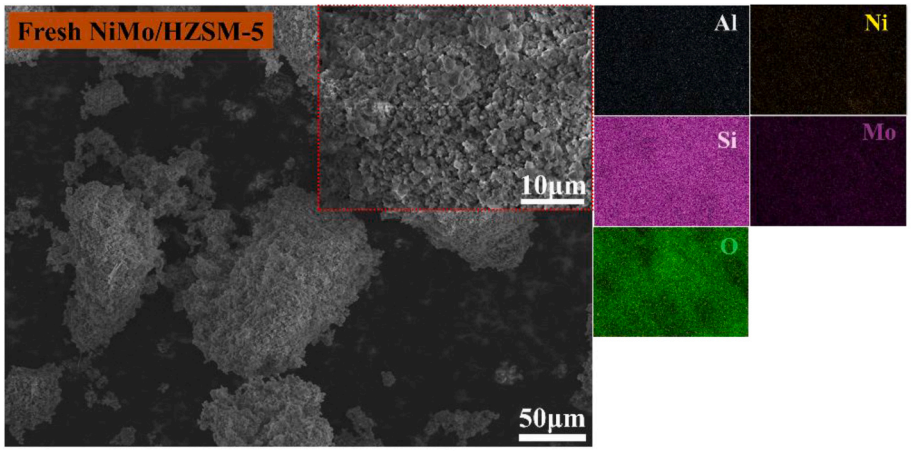

(c)

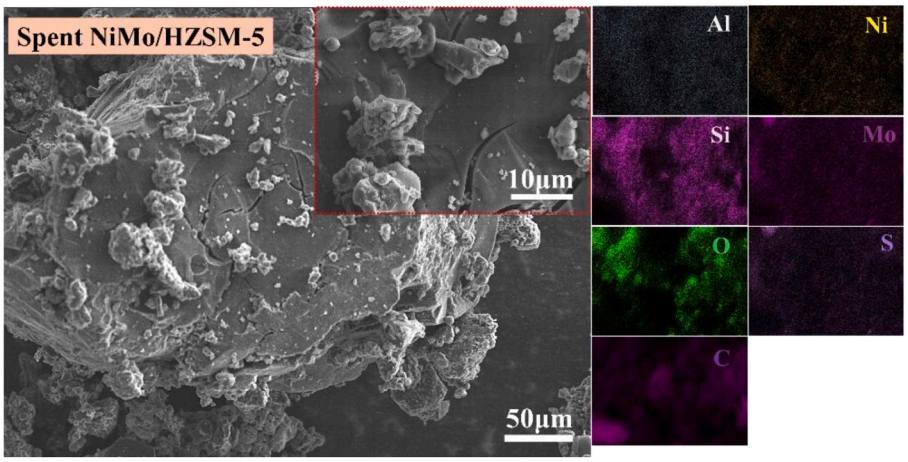

(d)

Fig. 4. (*continued*).

significant coke formation. The spent NiMo/Al_2O_3 and NiMo/HZSM-5 catalysts showed weight losses of 39 % and 53 %, respectively. The stability of NiMo catalysts on different supports decreases in the following order: self-prepared ZrO_2 > Al_2O_3 > HZSM-5, which responds to weight loss from coke deposition. The HZSM-5 had the highest coke content because it generated aromatic compounds in the liquid phase at high reaction temperatures. This is because some compounds could have cracked and converted to aromatics at strong acid sites [49]. On the other hand, ZrO_2 had the lowest coke content because the oxygen vacancies on ZrO_2 could promote the oxidation of deposited coke [50]. Therefore, the TGA results highlight the crucial role of coke deposition in determining catalyst performance and longevity. NiMo/ZrO_2 demonstrated superior stability with minimal coke formation, leading to extended catalyst life and reduced operational costs. Conversely, NiMo/Al_2O_3 and NiMo/HZSM-5 exhibited significantly higher coke deposition, which could result in more frequent catalyst regeneration and increased maintenance expenses. These findings emphasize the importance of choosing catalyst supports that offer a balance of activity, selectivity, and stability, ultimately improving both the performance and economic viability of biofuel production processes at an industrial scale.

3.2. Palm oil deoxygenation under glycerol as a hydrogen donor

3.2.1. Liquid products

It is well established that Al_2O_3 and HZSM-5 supports are widely used catalysts in deoxygenation processes. In this study, the performance of self-prepared ZrO_2 as a support for palm oil deoxygenation using glycerol as a hydrogen donor was compared with these two commercial supports. Reactions were conducted at 400 °C for 1 and 3 h. The results including elemental analysis, reaction evaluation (percent of carbon yield, oxygen removal, and alkane selectivity), and the properties of the liquid products (TAN and HHV), are presented in Table 3. A control experiment without a catalyst (blank test) was performed to assess the role of the catalyst, with the results described in our previous publication [17]. Palm oil deoxygenation with glycerol as a hydrogen donor in the absence of a catalyst showed maximum values at 400 °C for 3 h, with 65.9 % oxygen removal and 59.9 % alkane selectivity. As seen in Table 3, the use of the three catalysts significantly enhanced deoxygenation performance by markedly increasing oxygen removal and alkane selectivity. Thus, NiMo supported on commercial Al_2O_3, HZSM-5, and self-prepared ZrO_2 had a strong influence on this reaction.

As shown in Table 3, although palm oil contains high carbon content and a high HHV along with low TAN and oxygen content, it still requires transformation to be suitable for use as a transportation fuel. Palm oil is a triglyceride compound, which hinders efficient air mixing in combustion chambers, leading to poor fuel atomization. Additionally, its high viscosity makes it unsuitable for direct use as fuel without further processing [51].

At 1 h of reaction time, NiMo/Al_2O_3 achieved the highest C yield at 86.0 %, while NiMo on ZrO_2 and HZSM-5 produced similar C yields (as

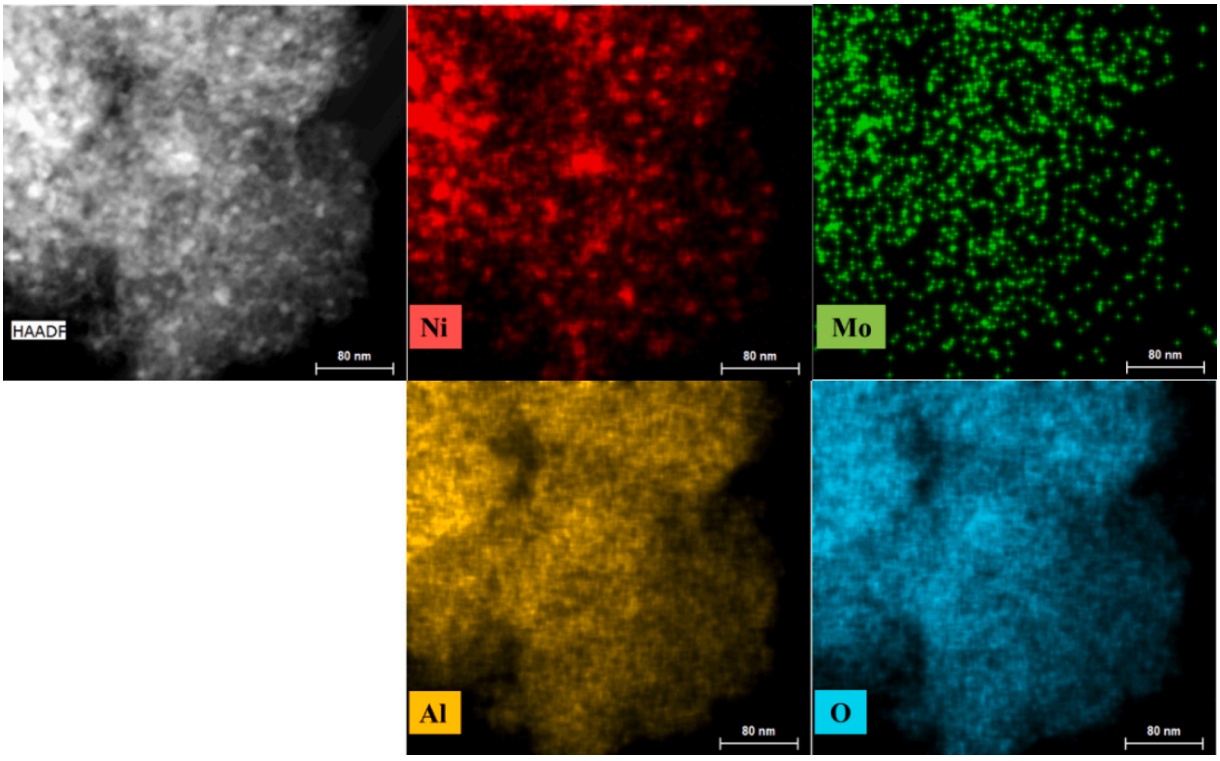

(a)

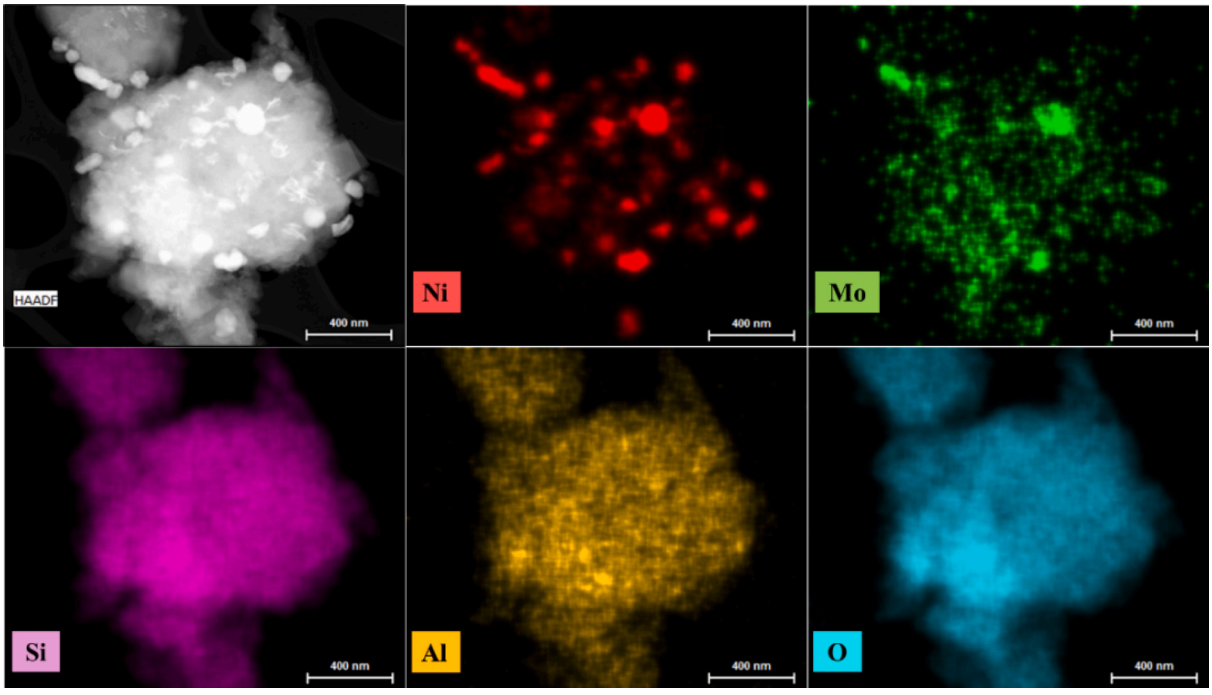

(b)

Fig. 5. Dark-field STEM image and EDS mapping of (a) NiMo/Al_2O_3 and (b) NiMo/HZSM-5.

shown in Table 3). The lower carbon yields were attributed to reduced liquid yield (as shown in Table S1), indicating carbon in palm oil loss to gas products due to decarboxylation, decarbonylation, and gas-phase reactions. The oxygen removal rates at 1 h of reaction were comparable across all three catalysts, but there were differences in alkane selectivity. NiMo/ZrO_2 exhibited the lowest alkane selectivity (68.8 %) and retained higher amounts of free fatty acids after triglyceride hydrogenolysis [52], suggesting that the self-prepared ZrO_2 may

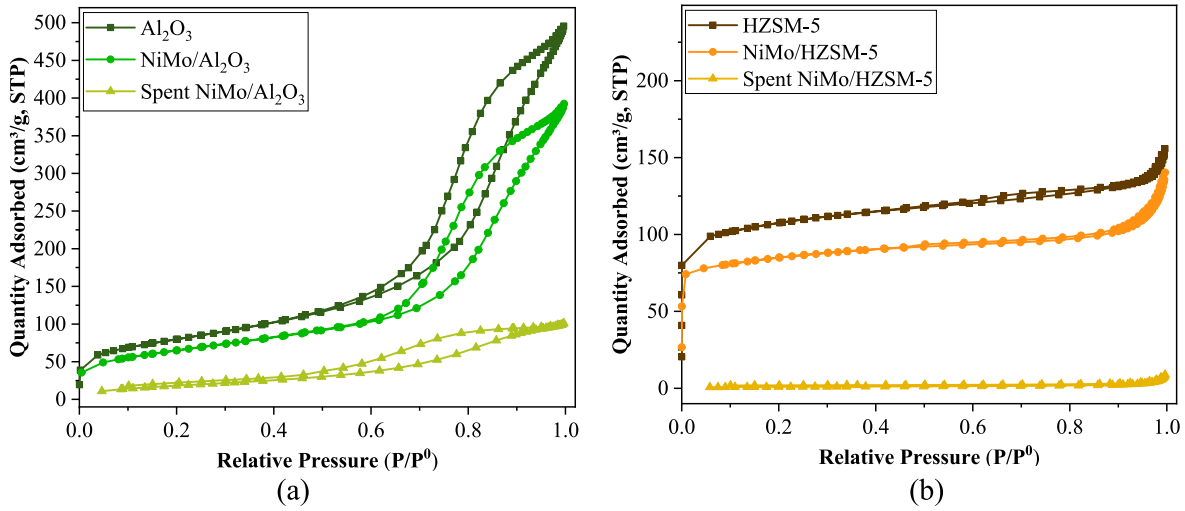

Fig. 6. N_2 adsorption-desorption isotherm of (a) NiMo on Al_2O_3 and (b) NiMo on HZSM-5.

Table 2
Textural properties of supports, fresh, and spent catalysts.

Sample	BET surface area (m^2/g)	Total pore volume (cm^3/g)
HZSM-5	377.0	0.09
NiMo/HZSM-5	325.0	0.11
Spent-NiMo/HZSM-5	3.0	0.01
Al_2O_3	285.0	0.79
NiMo/Al_2O_3	233.0	0.61
Spent-NiMo/ Al_2O_3	71.0	0.16

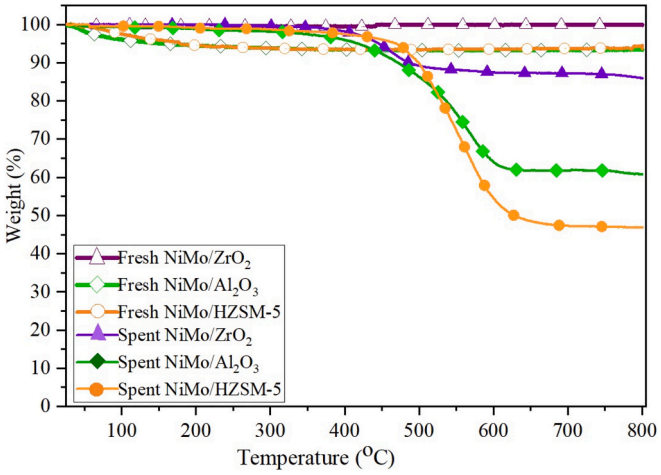

Fig. 7. TGA profile of fresh and spent catalysts.

exhibit slower catalytic activity for palm oil deoxygenation than Al_2O_3 and HZSM-5. However, an extended reaction time was necessary, as the results of 1 h for all catalysts were unsatisfactory.

The results of extending the reaction time from 1 to 3 h are presented in Table 3. For all catalysts, an increase in reaction time led to higher %C in the liquid product, while %O and %C yield decreased, indicating enhanced oxygen removal and cracking. These findings are consistent with the carbon distribution observed in Fig. 8 from GC–MS analysis, which showed that longer reaction times resulted in the production of lighter alkanes due to increased cracking [53]. At 3 h of reaction, the carbon and oxygen content in the liquid products, as well as carbon yield, appeared similar for NiMo/ZrO_2, NiMo/Al_2O_3, and NiMo/HZSM-5. NiMo/Al_2O_3 still exhibited the highest %C yield, but with no significant difference compared to other catalysts due to its higher liquid yield, suggesting limited oxygen removal and cracking. However, NiMo/Al_2O_3 had the lowest oxygen removal and alkane selectivity, while NiMo/ZrO_2 and NiMo/HZSM-5 showed comparable results. The highest oxygen removal was achieved with NiMo/ZrO_2 at 75.7 %, and the highest alkane selectivity was observed with NiMo/HZSM-5 at 95.9 %. The variations in oxygen removal were linked to the remaining oxygen content in the palm oil (triglyceride) and palm oil hydrolysates (free fatty acids) [52]. This suggests that the triglyceride content in palm oil remained higher with NiMo/HZSM-5 compared to NiMo/ZrO_2, indicating that NiMo/ZrO_2 had a higher efficiency in converting both triglycerides and free fatty acids into alkane hydrocarbons. Overall, NiMo/Al_2O_3 demonstrated the lowest performance compared to NiMo/ZrO_2 and NiMo/HZSM-5. This difference can be attributed to the substantial water produced within the reactor as a result of gas-phase reactions and the hydrodeoxygenation pathway [35]. The presence of water may hinder the performance of Al_2O_3, as strong water adsorption on its surface can suppress its active sites. When water interacts with the surface of Al_2O_3, it can lead to the formation of hydroxyl groups (–OH) on the catalyst surface. These hydroxyl groups can occupy active sites and alter the electronic properties of the surface, thereby hindering the catalyst's performance in palm oil deoxygenation [18]. This effect is evident from the slight decrease in fatty acid content and the corresponding increase in oxygen removal observed for NiMo/Al_2O_3 as the reaction time was extended from 1 to 3 h. In contrast, ZrO_2 and HZSM-5 exhibited greater resistance to water deactivation, as both oxygen removal and alkane selectivity continued to increase with longer reaction times.

The mechanisms for catalyzing the deoxygenation process differ between ZrO_2 and HZSM-5. In ZrO_2, oxygen vacancies play a crucial role in the reaction by providing active sites that facilitate the adsorption and activation of reactants. The formation of these vacancies, often through the removal of oxygen atoms, results in charge compensation within the material, enhancing its catalytic properties. When reactants adsorb onto these surface vacancies, C—O bonds are activated and subsequently cleaved, releasing byproducts such as carbon monoxide and carbon dioxide. This process not only increases the reactivity of ZrO_2 but also allows for continuous catalytic activity, making it an effective catalyst for deoxygenation reactions [36,54].

HZSM-5, on the other hand, has two types of acid sites: Lewis and Brønsted acid sites. Lewis acid sites act as electron acceptors, while Brønsted acid sites function as proton donors [19]. The mechanism involving these acid sites is illustrated in Fig. 9. The deoxygenation mechanism over HZSM-5 involves the synergistic actions of both

Table 3
Elemental composition, evaluation of reaction performance, and properties of liquid products using NiMo on different supports.

Catalyst	Reaction time (h)	Elemental analysis (%)***				Calculation (%)			Properties	
		C	H	S	O*	C yield	Oxygen removal	Alkane selectivity**	TAN (mg KOH/g)	HHV (MJ/kg)
Palm oil		76.9	12.5		10.6				1.05	39.3
Glycerol		38.5	9.1		52.4				0.00	17.8
$NiMo/ZrO_2$ [17]	1	76.7 ± 0.4	11.3 ± 0.7	0.5 ± 0.5	11.5 ± 0.4	79.6 ± 0.4	64.3 ± 1.4	68.8 ± 1.3	50.7 ± 2.0	39.9 ± 0.2
	3	79.4 ± 0.5	12.2 ± 0.1	0.1 ± 0.1	8.2 ± 0.6	79.0 ± 0.5	75.7 ± 1.8	92.9 ± 1.1	32.0 ± 0.1	42.2 ± 0.2
$NiMo/Al_2O_3$	1	76.5 ± 0.3	11.9 ± 0.0	0.5 ± 0.1	11.1 ± 0.2	86.0 ± 0.3	62.8 ± 0.7	81.9 ± 1.1	77.2 ± 0.2	39.6 ± 0.1
	3	77.5 ± 0.5	11.9 ± 0.1	0.3 ± 0.1	10.2 ± 0.2	80.5 ± 0.5	68.5 ± 1.9	85.9 ± 2.5	46.7 ± 0.5	41.3 ± 0.6
NiMo/HZSM5	1	76.4 ± 0.3	11.6 ± 0.2	0.7 ± 0.1	11.2 ± 0.2	79.4 ± 0.3	65.3 ± 0.5	88.4 ± 2.3	59.5 ± 1.1	40.1 ± 0.3
	3	78.7 ± 0.1	12.1 ± 0.1	0.5 ± 0.1	8.6 ± 0.1	78.4 ± 0.1	74.3 ± 0.2	95.9 ± 0.0	31.7 ± 1.2	41.7 ± 0.4

* By difference.
** The liquid product consists of fatty acids and alkane hydrocarbons.
*** %N less than 0.1 for all case.

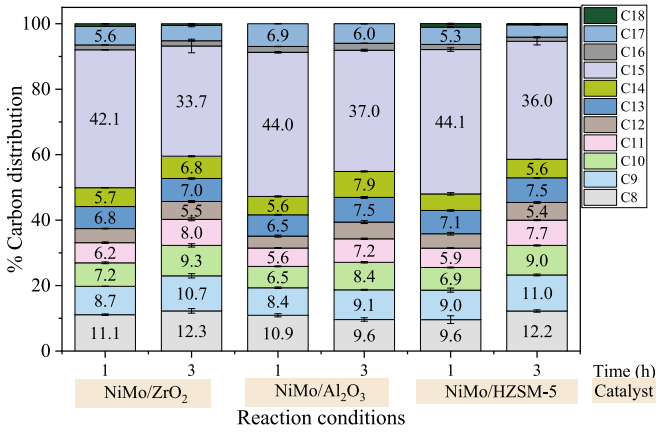

Fig. 8. The carbon distribution in liquid products using different catalysts at 400 °C.

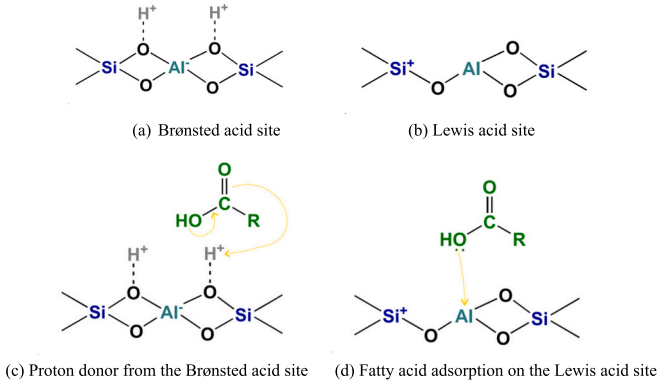

Fig. 9. The characteristics of acid sites on HZSM-5.

Brønsted and Lewis acid sites. Oxygenated compounds are adsorbed into the unique pore structure of HZSM-5 and are then protonated at the Brønsted acid sites, leading to the formation of reactive intermediates. The Lewis acid sites stabilize these intermediates and facilitate C—C bond formation. This activation step weakens C—O bonds, resulting in their cleavage and the formation of hydrocarbons, which are subsequently desorbed [19]. Furthermore, as an electron acceptor, the Lewis acid sites can enhance oxygen adsorption, leading to increased oxygen removal [55,56]. Although the acidity of HZSM-5 is highly beneficial for catalysis, coke deactivation can occur easily at high reaction temperatures as aromatic compounds form on the acid sites [57]. The experimental findings showed that small quantities of aromatic compounds were present when using NiMo/HZSM-5, which were not detected with the other catalysts. The existence of aromatic compounds correlated with the stability of NiMo/HZSM-5, as evidenced by the TGA (as shown in Fig. 7). NiMo/HZSM-5 exhibited the lowest stability due to coking deactivation, approximately 53 %.

The main components of the liquid product consist of alkane hydrocarbons with varying carbon chain lengths and fatty acids. The distribution of carbon number in liquid products using different catalysts at 400 °C is illustrated in Fig. 8. The results indicated that the carbon content of alkanes ranged between C_8 and C_{18}, with $C_{15}H_{32}$ being a major component in all cases. Longer alkanes ($>C_{15}$) appeared as the primary component, potentially suitable for the hydrocarbon range of jet fuel and diesel fuel [58]. With increased reaction time, the production of lighter alkanes intensified. Lighter alkanes (C_8-C_{14}) exhibited an increased production order of $NiMo/Al_2O_3$ < NiMo/HZSM-5 ≈ $NiMo/ZrO_2$. Moreover, NiMo/HZSM-5 and $NiMo/ZrO_2$ demonstrated similar capabilities in producing carbon distribution in liquid products. Another contributing factor to the decreased performance of Al_2O_3 in cracking was its moderate acidity [59]. Strong acid sites typically facilitate more cracking reactions [19], implying that Al_2O_3 may not be optimal for producing gasoline or jet fuel hydrocarbons, but it could be suitable for green diesel production. These findings are consistent with Dada et al. (2022), who studied the effect of mono (SrO) and bimetallic (Cu-SrO) catalysts over different catalyst supports (HZSM-5, Y-zeolite, activated carbon, Al_2O_3, and ZrO_2) on co-pyrolysis of biomass (ironbark) and waste cooking oil. Their research showed that both SrO and Cu-SrO on HZSM-5 and Y-zeolite exhibited similar behavior, promoting cracking reactions that produced lighter alkane hydrocarbons (C < 14) and reducing the formation of compounds with more than 20 carbon atoms compared to other supports, due to the strong acid sites on the HZSM-5 catalyst [60].

TAN and HHV are important indicators of the quality and stability of biofuel produced via the deoxygenation of palm oil. Table 3 presents the TAN and HHV values of both palm oil and the liquid products obtained from various catalysts. Palm oil has a low TAN and high HHV due to its high carbon content in the form of triglyceride structures and low oxygen content. The liquid products from all catalysts exhibited higher TAN

and HHV than palm oil. The increase in TAN is attributed to the fatty acids produced during the hydrogenolysis of palm oil and the formation of fatty acids reduces HHV [28]. However, the overall increase in HHV of liquid products for all cases is driven by the production of alkane hydrocarbons.

As the reaction time increases, TAN decreases across all catalyst systems ($NiMo/ZrO_2$, $NiMo/Al_2O_3$, and NiMo/HZSM-5), reflecting the ongoing deoxygenation process. For instance, at 3 h, the NiMo/HZSM-5 and $NiMo/ZrO_2$ catalysts significantly reduced TAN compared to 1 h, demonstrating their ability to efficiently remove oxygen from fatty acids and convert them into hydrocarbons. The highest remaining fatty acid content at 3 h for $NiMo/Al_2O_3$ resulted in lower TAN and HHV compared to $NiMo/ZrO_2$ and NiMo/HZSM-5.

The HHV of the liquid product tends to increase with longer reaction times. This is because the production of an energy-rich alkane hydrocarbon is associated with prolonged reaction times. Alkanes have higher HHVs than fatty acids due to their greater hydrogen-to-carbon ratio and lower oxygen content [61]. The increase in HHV over time reflects the improved conversion of oxygenates into alkane hydrocarbons, enhancing the biofuel's energetic density and making it more comparable to conventional fuels. $NiMo/ZrO_2$ and NiMo/HZSM-5 exhibited similar TAN and HHV values, which aligns with the results from GC–MS and CHNS-O analyses that demonstrated high alkane selectivity and effective oxygen removal. According to Jet A and Jet A1 standards, the HHV value is 42.8 MJ/kg [62]. Our highest recorded HHV result was 42.2 MJ/kg, which is close to the ASTM standard. Therefore, it appears that $NiMo/ZrO_2$ exhibited the best performance for palm oil deoxygenation using glycerol as a hydrogen donor for two primary reasons. First, $NiMo/ZrO_2$ demonstrated superior performance in terms of oxygen removal and alkane production. Second, $NiMo/ZrO_2$ exhibited the best stability, which was attributed to its lowest coke deactivation, as determined from the TGA analysis (as shown in Fig. 7).

While $NiMo/ZrO_2$ demonstrates superior performance in terms of oxygen removal, alkane selectivity, and resistance to coke formation, certain practical considerations should be noted. ZrO_2, despite its excellent thermal stability and ability to provide oxygen vacancies, may be more expensive and less readily available than Al_2O_3 and HZSM-5, which are commonly used commercial supports. The preparation of high-purity ZrO_2 with controlled properties may also require additional processing steps, increasing its overall production cost. These factors could limit its widespread adoption in industrial applications unless offset by its enhanced performance and longer catalyst lifespan, which could reduce the frequency of catalyst replacement. Future research could focus on developing strategies to reduce the cost of ZrO_2 production and improve its economic viability.

The performance of the catalysts in this study was compared to previous work reported in the literature. Khan et al. (2024) investigated palm oil deoxygenation using a 10 wt% Ni/ZSM-5-SAPO-11 catalyst at 350 °C and 60 bar H_2 for 2 h in a batch reactor, with a calculated WHSV (weight hourly space velocity, g feed/g catalyst•h) of 2.2. Their study resulted in a high alkane yield, predominantly in the jet fuel range, with the liquid product containing 77.2 % carbon, 12 % hydrogen, and a HHV of 43.38 MJ/kg [63]. Similarly, our study using a NiMo/HZSM-5 catalyst with a WHSV of 8 also produced alkanes in the jet fuel range, but with higher carbon (78.7 %) and hydrogen (12.1 %) contents, along with a comparable HHV of 41.7 MJ/kg after 3 h of reaction time. Although our reaction time was longer, the higher WHSV implies a shorter residence time for the palm oil on the catalyst surface, leading to a faster reaction rate [64], without the need for external hydrogen, as glycerol acted as a renewable hydrogen donor. Additionally, Tsiotsias et al. (2023) explored palm oil deoxygenation using a Ni/ZrO_2 catalyst at 300 °C and 30 bar H_2 for 20 h in a continuous reactor, reporting 95 % palm oil conversion and a 90 % alkane yield in the C8–C18 range [50]. In comparison, our $NiMo/ZrO_2$ catalyst achieved a similar alkane selectivity of 92.9 % in the C8–C18 range with a shorter reaction time and minimal coke formation. Another relevant comparison is Alwan et al. (2015), who studied biofuel production via oleic acid deoxygenation using glycerol as an in situ hydrogen donor. The reaction was carried out at 400 °C for 4 h using a NiWC/Al-SBA-15 catalyst, with a WHSV of 1.1. Their results showed 97.3 % oleic acid conversion with selectivity of 5.2 % and 13 % for C17 n-alkane and C17 alkene, respectively. Although our WHSV is higher than theirs, the results are comparable in terms of using glycerol as a hydrogen donor [65]. These comparisons underscore the efficiency and sustainability of our NiMo-based catalysts, particularly the use of glycerol as a hydrogen donor, which enhances the overall practicality and environmental compatibility of the process.

3.2.2. *The effect of catalyst on different fuel range production*

The catalytic performance of NiMo-based catalysts supported on different materials—ZrO_2, Al_2O_3, and HZSM-5—was assessed for fuel production using the SimDist technique. As illustrated in Fig. 10, the various fuel ranges produced by these catalysts show distinct product distributions. The reaction was carried out at 400 °C for 3 h. According to previous research, the $NiMo/ZrO_2$ catalyst yielded a product distribution of 18.2 % diesel, 45.5 % jet fuel, and 36.2 % gasoline, with jet fuel constituting the largest fraction [17]. In contrast, the $NiMo/Al_2O_3$ catalyst showed a higher selectivity towards diesel, producing 56.7 %, the highest among all catalysts studied. The alkane hydrocarbons in the jet fuel and gasoline ranges were produced at 20.8 % and 22.6 %, respectively, making it the catalyst with the lowest gasoline production. The NiMo/HZSM-5 catalyst generated 20.4 % diesel, slightly more than $NiMo/ZrO_2$ but less than $NiMo/Al_2O_3$, with jet fuel and gasoline production of 45.7 % and 33.9 %, respectively. The fuel range production of NiMo/HZSM-5 was comparable to that of the $NiMo/ZrO_2$ catalyst. This result was consistent with the carbon distribution observed in the liquid products. The active sites on $NiMo/ZrO_2$ and NiMo/HZSM-5 effectively promoted the formation of lighter alkanes through cracking [42,66], leading to the conversion of long-chain alkanes into shorter ones within the gasoline range. Conversely, $NiMo/Al_2O_3$, characterized by moderate acidity [42], exhibited a lower rate of cracking, resulting in a predominance of long-chain alkanes within the diesel fuel range as the primary product. These findings suggest that the support material plays a crucial role in determining the selectivity and efficiency of NiMo catalysts in the conversion process, significantly affecting the relative yields of diesel, jet fuel, and gasoline. Consequently, this study recommends $NiMo/Al_2O_3$ for green diesel production, while $NiMo/ZrO_2$ and NiMo/HZSM-5 are suggested for jet fuel production.

3.2.3. *Gas products*

The gas product composition from palm oil deoxygenation at 400 °C for 1 and 3 h, using glycerol as a hydrogen donor without a catalyst, primarily consisted of H_2, CO_2, CH_4, C_2H_6, and C_2H_4, with CO_2 being the dominant component, as reported in [17]. When using NiMo catalysts

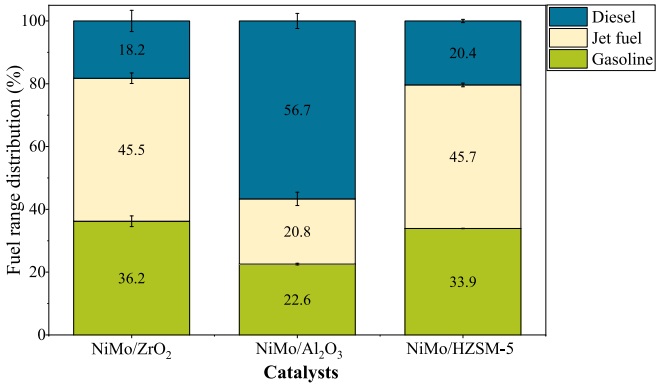

Fig. 10. The various fuel range production from palm oil deoxygenation from different catalysts.

on different supports under the same reaction conditions, as shown in Fig. 11, the resulting gas products displayed a similar composition, indicating that despite variations in catalysts and reaction times, the key gases produced remained consistent. This consistency can be attributed to the predominant occurrence of several key gas-phase reactions. H_2 was present despite not being introduced at the initial, indicating that glycerol can produce H_2 and confirming its role as a hydrogen donor. H_2, which is produced via glycerol decomposition and aqueous-phase reforming (APR), is a critical contributor to the process efficiency, as it acts as a renewable hydrogen source, reducing the dependence on externally supplied hydrogen. This self-sufficiency in hydrogen production can lower operational costs and improve the sustainability of the process. The deoxygenation of palm oil could potentially produce CO and CO_2 through decarbonylation and decarboxylation, respectively [37], but CO was not detected. Both CO and CO_2 are reactants in methanation reactions that produce CH_4 (as shown in Eq. (5) and (6)) [67]. CO methanation is favored over CO_2 methanation due to its more negative Gibbs free energy, making it more likely to occur [68]. Additionally, CO reacts in the water-gas shift reaction to form CO_2 and H_2 (as shown in Eq. (7)), a process that also happens due to the presence of H_2O from hydrodeoxygenation [69]. CO_2 was the most abundant gas across all experiments might be due to it being produced from both water gas shift and decarboxylation without further reaction. The complexity of the gas-phase reactions makes it challenging to correlate the gas-phase components with those in the liquid-phase reactions. The major gas phase reactions are listed below [68].

$$\text{CO methanation; } CO + 3H_2 \rightarrow CH_4 + H_2O \; \Delta G^{\circ}_{533} = -88.4 \text{ kJ/mol} \quad (5)$$

$$\text{CO_2 methanation; } CO_2 + 4H_2 \rightarrow CH_4 + 2H_2O \; \Delta G^{\circ}_{533} = -69.2 \text{ kJ/mol} \quad (6)$$

$$\text{Water gas shift; } CO + H_2O \rightarrow CO_2 + H_2 \quad (7)$$

Lighter hydrocarbons were generated through cracking [70]. CH_4 and other light hydrocarbons offer potential as energy carriers. These gases can be captured and utilized as fuel for heating the reactor or powering auxiliary systems, thereby enhancing the energy efficiency of the overall operation. For example, the energy content of CH_4 could significantly offset the energy demands of high-temperature reactions, reducing external energy inputs and improving process profitability. These gas products can improve process profitability by being integrated into circular economy strategies and utilized for energy recovery. By harnessing the energy potential of these gaseous byproducts, biofuel production can become more sustainable and economically viable, enhancing the overall efficiency and profitability of the process.

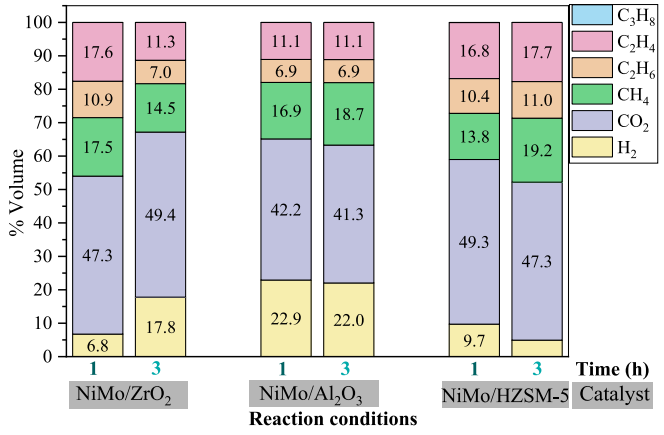

Fig. 11. Composition in gas phase products using NiMo on difference support at 400 °C.

3.2.4. *The proposed reaction pathway of palm oil deoxygenation using glycerol as a hydrogen donor over NiMo-based catalyst*

The proposed reaction pathway for palm oil deoxygenation using glycerol as a hydrogen donor over a NiMo-based catalyst is depicted in Fig. 12. This pathway describes the conversion of triglycerides in palm oil into alkane hydrocarbons through glycerol reactions, hydroprocessing in the liquid phase, and gas-phase reactions. The liquid product primarily consists of alkane hydrocarbons with varying carbon numbers, along with unreacted free fatty acids. The reaction mechanism can be described as follows;

Initially, glycerol undergoes decomposition and aqueous phase reforming (APR), producing CO, CO_2, and H_2 [71]. The hydrogen generated from glycerol can be utilized in liquid-phase reactions. Triglycerides are subjected to hydrogenolysis, breaking down into three fatty acids and propane (C_3H_8) [72]. These fatty acids are subsequently transformed into long-chain alkanes through deoxygenation, with the carbon number of the resulting alkanes corresponding to that of the original fatty acids. Three main reaction pathways of deoxygenation are observed: decarbonylation, in which fatty acids react with H_2, releasing CO and H_2O to form alkanes with one less carbon (R-H); decarboxylation, resulting in the release of CO_2 and the formation of alkanes with one fewer carbon (R-H); and hydrodeoxygenation, where fatty acids react with H_2, removing oxygen in form of H_2O and producing alkanes with the same carbon number as the original fatty acid (R-CH_3) [73,74]. The longer-chain alkanes produced can further undergo cracking, producing lighter alkane hydrocarbons suitable for use as jet fuel and gasoline [75]. Gas-phase reactions complement these processes by converting gases such as CO, CO_2, and H_2. Methanation reactions convert CO_2 and H_2 into CH_4 and H_2O, while the water-gas shift reaction generates additional H_2 through the reaction of CO with H_2O [74].

The reaction of pure glycerol with the NiMo/ZrO_2 catalyst was conducted at 400 °C for 3 h, resulting in the complete conversion of glycerol, with no residual glycerol detected in the final product. The primary products included water and gas-phase compounds, as illustrated in Fig. S2. The gas-phase composition consisted of H_2, CO, CH_4, CO_2, and light hydrocarbons. The formation of CO, CO_2, and H_2 was attributed to direct reactions involving glycerol, such as decomposition and APR [76]. Methanation reactions contributed to the production of CH_4 and water, while light hydrocarbon gases were generated through the hydrodeoxygenation of glycerol [77]. Consequently, in the deoxygenation of palm oil using glycerol as a hydrogen donor, the liquid-phase alkane hydrocarbons were exclusively derived from palm oil deoxygenation rather than glycerol conversion. The absence of glycerol peaks in the GC–MS analysis of the liquid phase confirmed its complete conversion. Ultimately, this integrated reaction pathway not only facilitates the efficient conversion of palm oil into valuable hydrocarbons but also maximizes the utilization of glycerol as a renewable hydrogen donor, enhancing the sustainability and economic viability of the process for biofuel production.

4. Conclusions

This study highlights the critical role of support materials in enhancing the performance of NiMo catalysts for palm oil deoxygenation using glycerol as a hydrogen donor. In our previous work, NiMo/ZrO_2 demonstrated superior performance for palm oil deoxygenation and stability with minimal coke formation. These attributes make it the most promising catalyst for efficient and sustainable biofuel production. In comparison, NiMo/A_2O_3 exhibited lower oxygen removal efficiency (68.5 %) due to water adsorption-induced deactivation, while NiMo/HZSM-5 showed high alkane selectivity but suffered significant coke formation (53 % weight loss). The choice of support also influenced the product range: NiMo/A_2O_3 is optimal for green diesel, whereas NiMo/ZrO_2 and NiMo/HZSM-5 are more suitable for jet fuel production.

The findings emphasize the industrial relevance of NiMo/ZrO_2 in achieving high-quality biofuels with improved catalyst longevity and

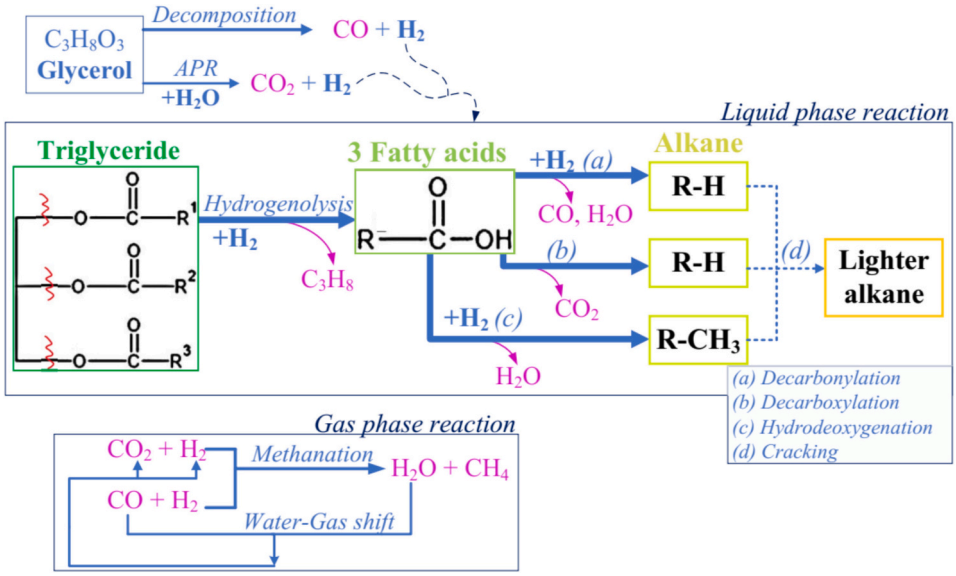

Fig. 12. The proposed reaction pathway of palm oil deoxygenation using glycerol as a hydrogen donor over NiMo-based catalyst.

reduced operational costs. These insights provide a foundation for designing advanced catalysts and optimizing renewable fuel production processes.

CRediT authorship contribution statement

Nitchakul Hongloi: Writing – review & editing, Writing – original draft, Methodology, Formal analysis, Data curation, Conceptualization. **Tawsif Rahman:** Writing – review & editing, Supervision, Methodology. **Farshad Feyzbar-Khalkhali-Nejad:** Writing – review & editing, Methodology, Data curation. **Chaiwat Prapainainar:** Writing – review & editing, Supervision. **Peerawat Wongsurakul:** Writing – review & editing, Writing – original draft, Methodology, Data curation. **Emmanuel Aransiola:** Writing – review & editing, Formal analysis, Data curation. **Lihua Zhang:** Writing – review & editing, Formal analysis, Data curation. **Pascal Bargiela:** Writing – review & editing, Formal analysis, Data curation. **Jonas Baltrusaitis:** Writing – review & editing, Data curation, Conceptualization. **Paweena Prapainainar:** Writing – review & editing, Supervision, Funding acquisition, Conceptualization. **Sushil Adhikari:** Writing – review & editing, Supervision, Funding acquisition, Conceptualization.

Declaration of competing interest

The authors declare that they have no known competing financial interests or personal relationships that could have appeared to influence the work reported in this paper.

Acknowledgments

Financial supports for this work were provided by the Alabama Department of Economic and Community Affairs (ADECA-1ARDEF22 02) and the Alabama Agricultural Experiment Station and the Hatch program (ALA014-1-19068). This research used Thermo Fisher Talos 200× of the Center for Functional Nanomaterials (CFN), which is a U.S. Department of Energy Office of Science User Facility at Brookhaven National Laboratory under Contract No. DE-SC0012704. The authors would like to thank the Faculty of Engineering, Kasetsart University, Bangkok, Thailand, and the National Center of Excellence for Petroleum, Petrochemicals, and Advanced Materials (PETROMAT). The authors acknowledge the Office of National Higher Education Science Research and Innovation Policy Council – PMU C, PTT Exploration and Production Public Co., Ltd., Cherdchai Corporation Co., Ltd., Polawat Engine Co., Ltd., and Verasuwan Co., Ltd. (C10F640103) for funding support. This project is also funded by the National Research Council of Thailand (NRCT) and Kasetsart University Research and Development Institute (KURDI), Kasetsart University (N42A670576). The author (NH) would like to thank Dr. Worapon Kiatkittipong for his support in recommending her as a visiting scholar at Auburn University.

Appendix A. Supplementary data

Supplementary data to this article can be found online at https://doi.org/10.1016/j.fuproc.2025.108196.

Data availability

Data will be made available on request.

References

[1] H. Singh, C. Li, P. Cheng, X. Wang, Q. Liu, A critical review of technologies, costs, and projects for production of carbon-neutral liquid e-fuels from hydrogen and captured CO2, Energy Adv. 1 (2022) 580–605, https://doi.org/10.1039/d2ya00173j.
[2] R.K. Srivastava, N.P. Shetti, K.R. Reddy, E.E. Kwon, M.N. Nadagouda, T. M. Aminabhavi, Biomass utilization and production of biofuels from carbon neutral materials, Environ. Pollut. 276 (2021) 116731, https://doi.org/10.1016/j.envpol.2021.116731.
[3] X.Y. Ooi, W. Gao, H.C. Ong, H.V. Lee, J.C. Juan, W.H. Chen, K.T. Lee, Overview on catalytic deoxygenation for biofuel synthesis using metal oxide supported catalysts, Renew. Sust. Energ. Rev. 112 (2019) 834–852, https://doi.org/10.1016/j.rser.2019.06.031.
[4] N. Hongloi, P. Prapainainar, C. Prapainainar, Review of green diesel production from fatty acid deoxygenation over Ni-based catalysts, Mol. Catal. 523 (2022) 111696, https://doi.org/10.1016/j.mcat.2021.111696.
[5] K. Hengst, M. Arend, R. Pfützenreuter, W.F. Hoelderich, Deoxygenation and cracking of free fatty acids over acidic catalysts by single step conversion for the production of diesel fuel and fuel blends, Appl. Catal. B Environ. 174-175 (2015) 383–394, https://doi.org/10.1016/j.apcatb.2015.03.009.
[6] C. Jia, C. Zhang, S. Xie, W. Zhang, Z. Wang, H. Lin, One-pot production of jet fuels from fatty acids and vegetable oils in biphasic tandem catalytic process, Fuel 302 (2021) 121060, https://doi.org/10.1016/j.fuel.2021.121060.
[7] N. Arun, R.V. Sharma, A.K. Dalai, Green diesel synthesis by hydrodeoxygenation of bio-based feedstocks: strategies for catalyst design and development, Renew. Sust. Energ. Rev. 48 (2015) 240–255, https://doi.org/10.1016/j.rser.2015.03.074.
[8] I. Hachemi, K. Jeništová, P. Mäki-Arvela, N. Kumar, K. Eränen, J. Hemming, D. Y. Murzin, Comparative study of sulfur-free nickel and palladium catalysts in hydrodeoxygenation of different fatty acid feedstocks for production of biofuels, Catal. Sci. Technol. 6 (2016) 1476–1487, https://doi.org/10.1039/C5CY01294E.

[9] S. Lycourghiotis, E. Kordouli, K. Bourikas, C. Kordulis, A. Lycourghiotis, The role of promoters in metallic nickel catalysts used for green diesel production: a critical review, Fuel Process. Technol. 244 (2023) 107690, https://doi.org/10.1016/j.fuproc.2023.107690.
[10] C. Yang, W. Wang, D. Wang, M. Gong, Y. Xin, L. Xiao, O.V. Kikhtyanin, D. Kubicka, W. Wu, The promotion effects of MoOx species in the highly effective NiMo/MgAl2O4 catalysts for the hydrodeoxygenation of methyl palmitate, J. Environ. Chem. Eng. 10 (2022) 107761, https://doi.org/10.1016/j.jece.2022.107761.
[11] H. Chang, G. Abdulkareem-Alsultan, Y.H. Taufiq-Yap, S. Mohd Izham, S. Sivasangar, Development of porous MIL-101 derived catalyst application for green diesel production, Fuel 355 (2024) 129459, https://doi.org/10.1016/j.fuel.2023.129459.
[12] M. Savarese, G. Castellini, M. Paleologo, G. Graffigna, Determinants of palm oil consumption in food products: a systematic review, J. Funct. Foods 96 (2022) 105207, https://doi.org/10.1016/j.jff.2022.105207.
[13] K.M. Isa, T.A.T. Abdullah, U.F.M. Ali, Hydrogen donor solvents in liquefaction of biomass: a review, Renew. Sust. Energ. Rev. 81 (2018) 1259–1268, https://doi.org/10.1016/j.rser.2017.04.006.
[14] P. Sharma, C.T. Avedisian, J.D. Brunson, W. Tsang, Decomposition by film boiling heat transfer of glycerol, Int. J. Heat Mass Transf. 139 (2019) 873–880, https://doi.org/10.1016/j.ijheatmasstransfer.2019.05.005.
[15] J. Wang, X. Yao, Y. Li, J. Zhang, C. Zhao, T.J. Strathmann, Catalytic hydrothermal deoxygenation of stearic acid with Ru/C: effects of alcohol- and carboxylic acid-based hydrogen donors, ACS Omega 8 (2023) 19969–19975, https://doi.org/10.1021/acsomega.3c01975.
[16] X. Besse, Y. Schuurman, N. Guilhaume, Hydrothermal conversion of linoleic acid and ethanol for biofuel production, Appl. Catal. A Gen. 524 (2016) 139–148, https://doi.org/10.1016/j.apcata.2016.06.030.
[17] T.R. Nitchakul Hongloi, Bijoy Biswas, Farshad Feyzbar-Khalkhali-Nejad, Chaiwat Prapainainar, Peerawat Wongsurakul, Pavlo Ivanchenko, Deb P. Jaisi, Emmanuel Aransiola, Lihua Zhang, Mohamed Ammar, Jonas Baltrusaitis, Paweena Prapainainar, Sushil Adhikari, Biofuel production from palm oil deoxygenation using nickel-molybdenum on zirconia catalyst using glycerol as a hydrogen donor, Energy Convers. Manag. X 24 (2024) 100781, https://doi.org/10.1016/j.ecmx.2024.100781.
[18] A.M. Hilmen, D. Schanke, K.F. Hanssen, A. Holmen, Study of the effect of water on alumina supported cobalt Fischer–Tropsch catalysts, Appl. Catal. A Gen. 186 (1999) 169–188, https://doi.org/10.1016/S0926-860X(99)00171-4.
[19] B. Valle, R. Palos, J. Bilbao, A.G. Gayubo, Role of zeolite properties in bio-oil deoxygenation and hydrocarbons production by catalytic cracking, Fuel Process. Technol. 227 (2022) 107130, https://doi.org/10.1016/j.fuproc.2021.107130.
[20] M. Aslam, Transformation of 1-G and 2-G liquid biomass to green fuels using hydroprocessing technology: a promising technology for biorefinery development, Biomass Bioenergy 163 (2022) 106510, https://doi.org/10.1016/j.biombioe.2022.106510.
[21] L. Sharma, J.P. Baltrus, S. Rangarajan, J. Baltrusaitis, Elucidating the underlying surface chemistry of Sn/Al2O3 catalysts during the propane dehydrogenation in the presence of H2S co-feed, Appl. Surf. Sci. 573 (2022) 151205, https://doi.org/10.1016/j.apsusc.2021.151205.
[22] M.P. Seah, Simple universal curve for the energy-dependent electron attenuation length for all materials, Surf. Interface Anal. 44 (2012) 1353–1359, https://doi.org/10.1002/sia.5033.
[23] J.H. Scofield, Hartree-Slater subshell photoionization cross-sections at 1254 and 1487 eV, J. Electron Spectrosc. Relat. Phenom. 8 (1976) 129–137.
[24] D.A. Shirley, High-resolution X-ray photoemission spectrum of the valence bands of gold, Phys. Rev. B 5 (1972) 4709–4714, https://doi.org/10.1103/PhysRevB.5.4709.
[25] G.H. Major, V. Fernandez, N. Fairley, M.R. Linford, A detailed view of the Gaussian–Lorentzian sum and product functions and their comparison with the Voigt function, Surf. Interface Anal. 54 (2022) 262–269, https://doi.org/10.1002/sia.7050.
[26] N. Fairley, V. Fernandez, M. Richard-Plouet, C. Guillot-Deudon, J. Walton, E. Smith, D. Flahaut, M. Greiner, M. Biesinger, S. Tougaard, D. Morgan, J. Baltrusaitis, Systematic and collaborative approach to problem solving using X-ray photoelectron spectroscopy, Appli. Surface Sci. Adv. 5 (2021) 100112, https://doi.org/10.1016/j.apsadv.2021.100112.
[27] H. Ojagh, D. Creaser, S. Tamm, P. Arora, S. Nyström, E. Lind Grennfelt, L. Olsson, Effect of dimethyl disulfide on activity of NiMo based catalysts used in hydrodeoxygenation of oleic acid, Ind. Eng. Chem. Res. 56 (2017) 5547–5557, https://doi.org/10.1021/acs.iecr.6b04703.
[28] H. Jahromi, S. Adhikari, P. Roy, E. Hassani, C. Pope, T.-S. Oh, Y. Karki, Production of green transportation fuels from Brassica carinata oil: a comparative study of noble and transition metal catalysts, Fuel Process. Technol. 215 (2021) 106737, https://doi.org/10.1016/j.fuproc.2021.106737.
[29] Y. Xu, G. Zhao, Q. Wang, Y. Zhan, B. Chen, Synthesis of Al2O3/SiO2 core–shell composite abrasives toward ultrasmooth and high-efficiency polishing for sapphire wafers, Proc. Inst. Mech. Eng., Part E 237 (2022) 1698–1708, https://doi.org/10.1177/09544089221124226.
[30] N. Subramanian, J. Vijaya, S. Sivasanker, R. Chinnadurai, S. Thangaraju Murugan, L. Kennedy, Hierarchical ZSM-5 catalytic performance evaluated in the selective oxidation of styrene to benzaldehyde using TBHP, J. Porous. Mater. 23 (2016), https://doi.org/10.1007/s10934-016-0129-8.
[31] A. Kostyniuk, D. Key, M. Mdleleni, Effect of Fe-Mo promoters on HZSM-5 zeolite catalyst for 1-hexene aromatization, J. Saudi Chem. Soc. 23 (2019) 612–626, https://doi.org/10.1016/j.jscs.2018.11.001.
[32] O. Rahmanpour, A. Shariati, M.R. Khosravi-Nikou, New method for synthesis nano size γ-Al2O3 catalyst for dehydration of methanol to dimethyl ether, Int. J. Chem. Eng. (2012) 125–128, https://doi.org/10.7763/IJCEA.2012.V3.172.
[33] A. Vedyagin, R. Kenzhin, M. Tashlanov, E. Alikin, V. Stoyanovskii, P. Plyusnin, Y. Shubin, I. Mishakov, M. Smirnov, A. Kalinkin, V. Bukhtiyarov, Effect of La addition on the performance of three-way catalysts containing palladium and rhodium, Top. Catal. 63 (2020), https://doi.org/10.1007/s11244-019-01213-x.
[34] M.B. Bahari, A.A. Jalil, C.R. Mamat, M.A. Arifin, N.S. Hassan, M. Alhassan, M. H. Sawal, N.M. Izzudin, A.H. Hatta, M.A. Aziz, D. Prasetyoko, S. Rajendran, Optimizing hydrogen-driven n-pentane isomerization over Pt-doped fibrous ZSM-5, Mol. Catal. 557 (2024) 113951, https://doi.org/10.1016/j.mcat.2024.113951.
[35] N. Hongloi, P. Prapainainar, A. Seubsai, K. Sudsakorn, C. Prapainainar, Nickel catalyst with different supports for green diesel production, Energy 182 (2019) 306–320, https://doi.org/10.1016/j.energy.2019.06.020.
[36] C. Zhao, W. Zhu, C. Liang, Role of ZrO2 crystal on the hydrodeoxygenation of methyl palmitate over NiMo/ZrO2 catalyst, Fuel 358 (2024) 130313, https://doi.org/10.1016/j.fuel.2023.130313.
[37] F. Shi, H. Wang, Y. Chen, Y. Lu, D. Hou, C. Liu, Y. Lu, X. Lin, X. Yang, Z. Zheng, Y. Zheng, Green diesel-like hydrocarbon production by H2-free catalytic deoxygenation of oleic acid via Ni/MgO-Al2O3 catalysts: effect of the metal loading amount, J. Environ. Chem. Eng. 11 (2023) 110520, https://doi.org/10.1016/j.jece.2023.110520.
[38] M.A. Abo El-Khair, S.A. Hanafi, M.G. Abd El-Moghny, M. El Saied, M.S. Elmelawy, M.S. El-Deab, Boosted Bio-Jet production: Unveiling the potential of a one-stage concurrent process of deoxygenation/upgrading versus two-stage sequential processes using Pt/Cl-Al2O3@Ni/ZSM-5 catalysts, Chem. Eng. J. 490 (2024) 151716, https://doi.org/10.1016/j.cej.2024.151716.
[39] D. Xiong, W. Li, L. Liu, Vertically aligned porous nickel(II) hydroxide nanosheets supported on carbon paper with long-term oxygen evolution performance, Chem. Asian J. 12 (2017) 543–551, https://doi.org/10.1002/asia.201601590.
[40] J. Baltrusaitis, B. Mendoza-Sanchez, V. Fernandez, R. Veenstra, N. Dukstiene, A. Roberts, N. Fairley, Generalized molybdenum oxide surface chemical state XPS determination via informed amorphous sample model, Appl. Surf. Sci. 326 (2015) 151–161, https://doi.org/10.1016/j.apsusc.2014.11.077.
[41] M. Thommes, K. Kaneko, A. Neimark, J. Olivier, F. Rodriguez-Reinoso, J. Rouquerol, K. Sing, Physisorption of gases, with special reference to the evaluation of surface area and pore size distribution (IUPAC Technical Report), Pure and Applied Chemistry 87 (9-10) (2015) 1051–1069, https://doi.org/10.1515/pac-2014-1117.
[42] M. Huang, L. Zhu, Z. Ma, Y. Yang, Highly selective production of light aromatics from lignin through integrated approach of the torrefaction deoxygenation pretreatment and the dual-catalyst catalytic fast pyrolysis using Nb modified γ-Al2O3 and HZSM-5, Fuel 354 (2023) 129318, https://doi.org/10.1016/j.fuel.2023.129318.
[43] T. Ramezani, S.M. Sadrameli, A. Bayat, A.H. Saeedi Dehaghani, Bio-gasoline and bio-naphtha production from catalytic cracking of linseed oil methyl ester over iron- and zinc-modified HZSM-5 and γ-Al2O3 catalysts in a fixed double-beds reactor, Fuel Process. Technol. 238 (2022) 107514, https://doi.org/10.1016/j.fuproc.2022.107514.
[44] A. Sokol, A. Beale, M. Sánchez-Sánchez, A. Sapi, U. Kashaboina, K. Ábrahámné, J. Gómez Pérez, S. Imre, G. Halasi, J. Kiss, B. Nagy, T. Varga, A. Kukovecz, Z. Kónya, Synergetic of Pt nanoparticles and H-ZSM-5 zeolites for efficient CO2 activation: role of interfacial sites in high activity, Front.Mater. 6 (2019) 127, https://doi.org/10.3389/fmats.2019.00127.
[45] H. Li, K. Sun, S. Xiong, W. Wang, W. Wu, Highly effective Pt-Pd/ZSM-22 catalysts prepared by the room temperature electron reduction method for the n-hexadecane hydroisomerization, Fuel Process. Technol. 262 (2024) 108117, https://doi.org/10.1016/j.fuproc.2024.108117.
[46] T.-S. Chen, L. Guo, H.-W. Peng, Y.-Q. Li, X.-B. Wang, H.-C. Bai, Z.-Y. Du, W.-Y. Li, Tuning support acidity of Ni-based catalysts to improve hydrodeoxygenation activity for dibenzofuran, Fuel Process. Technol. 236 (2022) 107440, https://doi.org/10.1016/j.fuproc.2022.107440.
[47] Ł. Szkudlarek, K. Chałupka-Śpiewak, W. Maniukiewicz, M. Nowosielska, J. Albińska, M.I. Szynkowska-Jóźwik, P. Mierczyński, CaO catalysts supported on ZSM-5 zeolite for biodiesel production via transesterification of rapeseed oil, Appl. Catal.O: Open 194 (2024) 206999, https://doi.org/10.1016/j.apcato.2024.206999.
[48] X. Dai, Y. Cheng, T. Liu, L. Mao, Deactivation mechanism of NiWS/SAPO-11 catalyst in hydroisomerization of n-hexadecane: Insights into coke deposition behavior and active phase migration, Fuel 375 (2024) 132614, https://doi.org/10.1016/j.fuel.2024.132614.
[49] P. Sirous Rezaei, H. Shafaghat, W.M.A.W. Daud, Suppression of coke formation and enhancement of aromatic hydrocarbon production in catalytic fast pyrolysis of cellulose over different zeolites: effects of pore structure and acidity, RSC Adv. 5 (2015) 65408–65414, https://doi.org/10.1039/C5RA11332F.
[50] A.I. Tsiotsias, S. Hafeez, N.D. Charisiou, S.M. Al-Salem, G. Manos, A. Constantinou, S. AlKhoori, V. Sebastian, S.J. Hinder, M.A. Baker, K. Polychronopoulou, M. A. Goula, Selective catalytic deoxygenation of palm oil to produce green diesel over Ni catalysts supported on ZrO2 and CeO2–ZrO2: Experimental and process simulation modelling studies, Renew. Energy 206 (2023) 582–596, https://doi.org/10.1016/j.renene.2023.02.038.
[51] S. Sidibe, J. Blin, T. Daho, G. Vaitilingom, J. Koulidiati, Comparative study of three ways of using Jatropha curcas vegetable oil in a direct injection diesel engine, Sci. Afr. 7 (2020) e00290, https://doi.org/10.1016/j.sciaf.2020.e00290.
[52] M. Žula, M. Grilc, B. Likozar, Hydrocracking, hydrogenation and hydrodeoxygenation of fatty acids, esters and glycerides: Mechanisms, kinetics and

transport phenomena, Chem. Eng. J. 444 (2022) 136564, https://doi.org/10.1016/j.cej.2022.136564.
[53] J. Asomaning, P. Mussone, D.C. Bressler, Thermal deoxygenation and pyrolysis of oleic acid, J. Anal. Appl. Pyrolysis 105 (2014) 1–7, https://doi.org/10.1016/j.jaap.2013.09.005.
[54] H. Chen, Y. Wu, S. Qi, Y. Chen, M. Yang, Deoxygenation of octanoic acid catalyzed by hollow spherical Ni/ZrO2, Appl. Catal. A Gen. 529 (2017) 79–90, https://doi.org/10.1016/j.apcata.2016.10.014.
[55] A. Popov, E. Kondratieva, J.M. Goupil, L. Mariey, P. Bazin, J.-P. Gilson, F. Maugé, Bio-oils hydrodeoxygenation: adsorption of phenolic molecules on oxidic catalyst supports, J. Phys. Chem. C 114 (2010) 15661–15670, https://doi.org/10.1021/jp101949j.
[56] Q. Zou, H. He, J. Xie, S. Han, W. Lin, A.K. Mondal, F. Huang, Study on the mechanism of acid modified H-Beta zeolite acidic sites on the catalytic pyrolysis of Kraft lignin, Chem. Eng. J. 462 (2023) 142029, https://doi.org/10.1016/j.cej.2023.142029.
[57] X. Zhao, L. Wei, J. Julson, Q. Qiao, A. Dubey, G. Anderson, Catalytic cracking of non-edible sunflower oil over ZSM-5 for hydrocarbon bio-jet fuel, New Biotechnol. 32 (2015) 300–312, https://doi.org/10.1016/j.nbt.2015.01.004.
[58] C. Collins, Implementing phytoremediation of petroleum hydrocarbons, in: Phytoremediation, 2007, pp. 99–108.
[59] X. Li, X. Ren, M. Wang, Q. Yang, Cascade hydrogenation of nitrobenzene to dicyclohexylamine with Pd/γ-Al2O3: the role of acid sites, Appl. Catal. A Gen. 644 (2022) 118835, https://doi.org/10.1016/j.apcata.2022.118835.
[60] T. Kassa Dada, A. Vuppaladadiyam, A. Xiaofei Duan, R. Kumar, E. Antunes, Probing the effect of Cu-SrO loading on catalyst supports (ZSM-5, Y-zeolite, activated carbon, Al2O3, and ZrO2) for aromatics production during catalytic co-pyrolysis of biomass and waste cooking oil, Bioresour. Technol. 360 (2022) 127515, https://doi.org/10.1016/j.biortech.2022.127515.
[61] N.A.A. Rahman, J. Fermoso, A. Sanna, Effect of Li-LSX-zeolite on the in-situ catalytic deoxygenation and denitrogenation of Isochrysis sp. microalgae pyrolysis vapours, Fuel Process. Technol. 173 (2018) 253–261, https://doi.org/10.1016/j.fuproc.2018.01.020.
[62] M. Mofijur, S.F. Ahmed, Z.I. Rony, K.S. Khoo, A.A. Chowdhury, M.A. Kalam, V. G. Le, I.A. Badruddin, T.M.Y. Khan, Screening of non-edible (second-generation) feedstocks for the production of sustainable aviation fuel, Fuel 331 (2023) 125879, https://doi.org/10.1016/j.fuel.2022.125879.
[63] S. Khan, K.M. Qureshi, Z. Luyao, A.N.K. Lup, M.F.A. Patah, C.Y. Chuah, W.M. A. Wan Daud, Jet fuel production via palm oil hydrodeoxygenation over bifunctional zeolite mixture supported Ni catalyst: effect of Si/Al ratio, Biomass Bioenergy 185 (2024) 107237, https://doi.org/10.1016/j.biombioe.2024.107237.
[64] E. Yoo, D.-S. Choi, J. Kim, Y.-H. Kim, N.-Y. Kim, J.B. Joo, Effects of operating parameters and feed gas compositions on the dry reforming of methane over the Ni/Al2O3 catalyst, in: Catalysts, 2023.
[65] B. Al Alwan, S.O. Salley, K.Y.S. Ng, Biofuels production from hydrothermal decarboxylation of oleic acid and soybean oil over Ni-based transition metal carbides supported on Al-SBA-15, Appl. Catal. A Gen. 498 (2015) 32–40, https://doi.org/10.1016/j.apcata.2015.03.012.
[66] S. Varimalla, K. Manda, S. Boggala, R.C. Nappuni, S. Inkollu, H.P. Aytam, V. Akula, Effect of method of preparation of Ni and/or Cu supported on ZSM-5 catalysts for the aqueous phase hydrogenation of levulinic acid to γ-valerolactone, Catal. Today 441 (2024) 114916, https://doi.org/10.1016/j.cattod.2024.114916.
[67] D. Schmider, L. Maier, O. Deutschmann, Reaction Kinetics of CO and CO2 Methanation over Nickel, Ind. Eng. Chem. Res. 60 (2021) 5792–5805, https://doi.org/10.1021/acs.iecr.1c00389.
[68] B. Peng, C. Zhao, S. Kasakov, S. Foraita, J.A. Lercher, Manipulating catalytic pathways: deoxygenation of palmitic acid on multifunctional catalysts, Chemistry 19 (15) (2013) 4732–4741, https://doi.org/10.1002/chem.201203110.
[69] M. Arend, T. Nonnen, W.F. Hoelderich, J. Fischer, J. Groos, Catalytic deoxygenation of oleic acid in continuous gas flow for the production of diesel-like hydrocarbons, Appl. Catal. A Gen. 399 (2011) 198–204, https://doi.org/10.1016/j.apcata.2011.04.004.
[70] D. Prangklang, D. Tumnantong, B. Yoosuk, C. Ngamcharussrivichai, P. Prasassarakich, Selective deoxygenation of waste cooking oil to diesel-like hydrocarbons using supported and unsupported NiMoS 2 catalysts, ACS Omega 8 (2023), https://doi.org/10.1021/acsomega.3c06188.
[71] V. Domínguez-Barroso, C. Herrera, M.Á. Larrubia, L.J. Alemany, Coupling of glycerol-APR and in situ hydrodeoxygenation of fatty acid to produce hydrocarbons, Fuel Process. Technol. 190 (2019) 21–28, https://doi.org/10.1016/j.fuproc.2019.03.011.
[72] A. Srifa, K. Faungnawakij, V. Itthibenchapong, S. Assabumrungrat, Roles of monometallic catalysts in hydrodeoxygenation of palm oil to green diesel, Chem. Eng. J. 278 (2015) 249–258, https://doi.org/10.1016/j.cej.2014.09.106.
[73] V. Itthibenchapong, A. Srifa, R. Kaewmeesri, P. Kidkhunthod, K. Faungnawakij, Deoxygenation of palm kernel oil to jet fuel-like hydrocarbons using Ni-MoS2/γ-Al2O3 catalysts, Energy Convers. Manag. 134 (2017) 188–196, https://doi.org/10.1016/j.enconman.2016.12.034.
[74] F. Zhao, Z. Chen, L. Hu, B. Wang, R. Zhang, Y. Yan, T. Jiang, Q. Jiang, C. Xu, Analysis of palm oil hydrodeoxygenation pathway selectivity based on oxygen quantification, Fuel Process. Technol. 252 (2023) 107950, https://doi.org/10.1016/j.fuproc.2023.107950.
[75] A. Afshar Taromi, S. Kaliaguine, Green diesel production via continuous hydrotreatment of triglycerides over mesostructured γ-alumina supported NiMo/CoMo catalysts, Fuel Process. Technol. 171 (2018) 20–30, https://doi.org/10.1016/j.fuproc.2017.10.024.
[76] C.A. Schwengber, H.J. Alves, R.A. Schaffner, F.A. da Silva, R. Sequinel, V.R. Bach, R.J. Ferracin, Overview of glycerol reforming for hydrogen production, Renew. Sust. Energ. Rev. 58 (2016) 259–266, https://doi.org/10.1016/j.rser.2015.12.279.
[77] V. Zacharopoulou, E.S. Vasiliadou, A.A. Lemonidou, One-step propylene formation from bio-glycerol over molybdena-based catalysts, Green Chem. 17 (2015) 903–912, https://doi.org/10.1039/C4GC01307G.